Applying Seismic Methods to National Security Problems:

Matched Field Processing With Geological Heterogeneity

Principal Investigator (PI): Phil Harben (ESD)
Coinvestigators:
Dave Harris (ESD)
Stephen Myers (ESD)
Shawn Larsen (Computations)
Jeff Wagoner (ESD)
Bruce Henderer (Engineering)
Dave McCallen (Engineering)
Jim Trebes (PAT)

October 29, 2003

Project 01-ERD-096

Applying Seismic Methods to National Security Problems:

Matched Field Processing With Geological Heterogeneity

Principal Investigator (PI): Phil Harben (ESD)
Coinvestigators:
Dave Harris (ESD)
Stephen Myers (ESD)
Shawn Larsen (Computations)
Jeff Wagoner (ESD)
Bruce Henderer (Engineering)
Dave McCallen (Engineering)
Jim Trebes (PAT)

Project 01-ERD-096

Contents

Executive Summary

Seismic imaging and tracking methods have intelligence and monitoring applications. Current systems, however, do not adequately calibrate or model the unknown geological heterogeneity. Current systems are also not designed for rapid data acquisition and analysis in the field. This project seeks to build the core technological capabilities coupled with innovative deployment, processing, and analysis methodologies to allow seismic methods to be effectively utilized in the applications of seismic imaging and vehicle tracking where rapid (minutes to hours) and real-time analysis is required. The goal of this project is to build capabilities in acquisition system design, utilization of full three-dimensional (3D) finite difference modeling, as well as statistical characterization of geological heterogeneity. Such capabilities coupled with a rapid field analysis methodology based on matched field processing are applied to problems associated with surveillance, battlefield management, finding hard and deeply buried targets, and portal monitoring. This project, in support of LLNL's national-security mission, benefits the U.S. military and intelligence community.

Fiscal year (FY) 2003 was the final year of this project. In the 2.5 years this project has been active, numerous and varied developments and milestones have been accomplished. A wireless communication module for seismic data was developed to facilitate rapid seismic data acquisition and analysis. The E3D code was enhanced to include topographic effects. Codes were developed to implement the Karhunen-Loeve (K-L) statistical methodology for generating geological heterogeneity that can be utilized in E3D modeling. The matched field processing methodology applied to vehicle tracking and based on a field calibration to characterize geological heterogeneity was tested and successfully demonstrated in a tank tracking experiment at the Nevada Test Site. A three-seismic- array vehicle tracking testbed was installed on site at LLNL for testing real-time seismic tracking methods. A field experiment was conducted over a tunnel at the Nevada Site that quantified the tunnel reflection signal and, coupled with modeling, identified key needs and requirements in experimental layout of sensors. A large field experiment was conducted at the Lake Lynn Laboratory, a mine safety research facility in Pennsylvania, over a tunnel complex in realistic, difficult conditions. This experiment gathered the necessary data for a full 3D attempt to apply the methodology. The experiment also collected data to analyze the capabilities to detect and locate in-tunnel explosions for mine safety and other applications.

In FY03 specifically, a large and complex simulation experiment was conducted that tested the full modeling-based approach to geological characterization using E2D, the K-L statistical methodology, and matched field processing applied to tunnel detection with surface seismic sensors. The simulation validated the full methodology and the need for geological heterogeneity to be accounted for in the overall approach. The Lake Lynn site area was geologically modeled using the code Earthvision to produce a 32 million node 3D model grid for E3D. Model linking issues were resolved and a number of full 3D model runs were accomplished using shot locations that matched the data. E3D-generated wavefield movies showed the reflection signal would be too small to be observed in the data due to trapped and attenuated energy in the weathered layer. An analysis of the few sensors coupled to bedrock did not improve the reflection signal

strength sufficiently because the shots, though buried, were within the surface layer and hence attenuated. Ability to model a complex 3D geological structure and calculate synthetic seismograms that are in good agreement with actual data (especially for surface waves and below the complex weathered layer) was demonstrated. We conclude that E3D is a powerful tool for assessing the conditions under which a tunnel could be detected in a specific geological setting. Finally, the Lake Lynn tunnel explosion data were analyzed using standard array processing techniques. The results showed that single detonations could be detected and located but simultaneous detonations would require a strategic placement of arrays.

Introduction

Seismic methods measure and analyze elastic wave vibrations propagating through the earth. The realm of application and specialization of seismic methods is enormous. The best-known and largest-scale is the application to worldwide seismic monitoring of large earthquakes (to determine location and source properties); also well-known is the application to monitor underground nuclear explosions (to identify and locate clandestine nuclear tests). On a smaller scale, active-source reflection seismology is used extensively by the oil industries for determining subsurface structure in the search for new oil prospects. Seismic methods have also been applied to problems of national security interest. Two such applications are the use of seismic methods to locate and track the movement of vehicles and the use of active or passive seismic methods to locate, identify, and characterize man-made underground structures, such as large tunnels and underground bunker complexes.

Although seismic networks that monitor earthquakes have become highly automated in the past decade, with earthquake location and source parameters available minutes to hours after an event, most seismic applications require long and laborious analysis. The reasons are generally tied to the applications and the requirements, as well as to the field equipment. In oil exploration, for example, hundreds of hardwired geophones record waveforms from a large number of active source locations. The recorded waveforms are later subjected to a complex and sophisticated series of processing and analysis steps to finally determine subsurface structure. The analysis is manpower and computer resource intensive and can take months to complete.

The use of seismic arrays to track vehicles and to characterize man-made underground structures for problems of national security interest is burdened with the same shortcomings as applications in other realms such as oil exploration. Equipment limitations and a robust processing strategy are currently limiting vehicle tracking applications. Wireless communication of seismic data to a central PC that analyzes and reliably maps the vehicle position within a monitored region in near-real time is the ultimate goal. However, reliable wireless utilization of seismic data has not been demonstrated in such a manner, and standard array processing methods have not proved reliable in tracking applications.

The application of seismic methods to underground facility characterization is very similar to the exploration field methods, except on a much smaller scale. The long processing and analysis time required between data acquisition and final result, however, is the same. In addition, a rapid deployment and assessment approach has not been tried to date. Past efforts have focused on large laborious proof-of-principle deployments over man-made structures in an attempt to produce detailed seismic images of the structure below. Analysis results followed the data collection by months to years.

Approach: The overall approach and objectives of this effort are best viewed as a capability-building project that combines technical advances with a data processing strategy to create a unique seismic monitoring capability for intelligence and security applications. The technical advances are: major enhancements to the E3D code to provide accurate wavefield models for sources in realistic topography and

complex heterogeneous geology; adaptation and application of state-of-the-art, self-configuring wireless network communications to seismic array and network deployments supporting real-time engagements; and a geophysical modeling paradigm supporting underground structure characterization and source location in uncertain, heterogeneous media. The processing strategy is the application of a matched field methodology to compare precomputed model data or calibrated field data with the incoming field data to quickly determine a "best match" between the field data and predetermined wavefield expectations. As mentioned before, the focus and uniqueness of this effort are on providing rapid assessments in real time or near-real time. We focus on two applications of interest to the user community: vehicle tracking with seismic arrays and detection/mapping of underground structures with active and passive seismic methods. This approach is unique in attempting to give real-time or near-real-time answers in the field, but it is not solving an imaging or tracking problem in an exact way. Rather, rapid analysis in the field is possible because the problem has been reduced to essentially choosing between a set of alternative hypotheses by using the field data to determine a best match. For underground facility characterization, this means alternate hypotheses on facility layout are used in wavefield simulations that are matched to the field data. The final outcome is a determination of the layout that best fits the field data. In vehicle tracking, the field data is windowed into small time increments (less than 1 sec) and each window is matched against the calibrated records from each grid point in the tracking area. The best grid point match is the vehicle location at that time.

This report details the technical capability-building accomplishments and the implementation of the full matched field methodology in two important national security applications: vehicle tracking and underground structure characterization. The vehicle tracking application resulted in two distinct field experiments: a tank tracking deployment at the Nevada Test Site and an LLNL site deployment in the vicinity of Building 170. The underground structure characterization application resulted in two field experiments and a computer simulation experiment. The first field experiment was a simple 2D experiment over a tunnel at the Nevada Test Site. The second field experiment was a large deployment at the Lake Lynn mine safety research facility in Pennsylvania.

Technology Development

Specific capability-building technical developments were essential for this project to achieve stated objectives in the application of the overall methodology to real world examples. The three developments that were funded, in part or fully by this project, were: implementation of topography in E3D, advances in wireless communication, and application coding of the Karhunen-Loeve (K-L) method for implementing geological heterogeneity. This section will briefly detail the successful technical developments of each.

Topography in E3D: The 3D finite difference full wavefield elastic propagation code named E3D has become an important LLNL research tool on a wide variety of applications and projects and is the state of the art in finite difference wavefield simulation codes (Larsen, 1998). It is a core capability required to generate the simulated data needed in the application of matched field processing (MFP) using a model-based approach. For the tunnel detection application, E3D is crucial, but had a major shortcoming. Most underground facilities and underground facility detection test areas are in hilly terrain. Considering the small scale, the topographic effects on the measured wavefield are significant and, if not accounted for, could overwhelm any signal differences arising from different subsurface structures. E3D did not have the capability to account for topographic effects on the wavefield prior to the start of this project. Significant effort was spent building the fundamental extensions to E3D so that topography could be included in the input model and accurate wavefields could be calculated that would account for the topographic effects. The E3D development was accomplished in FY02 so that the new capability could be utilized in FY03. Figure 1 shows a calculation using the enhanced E3D to demonstrate the effect topography has on the character of the wave propagation. The topographic enhancements were used extensively in the Lake Lynn modeling, as will be shown.

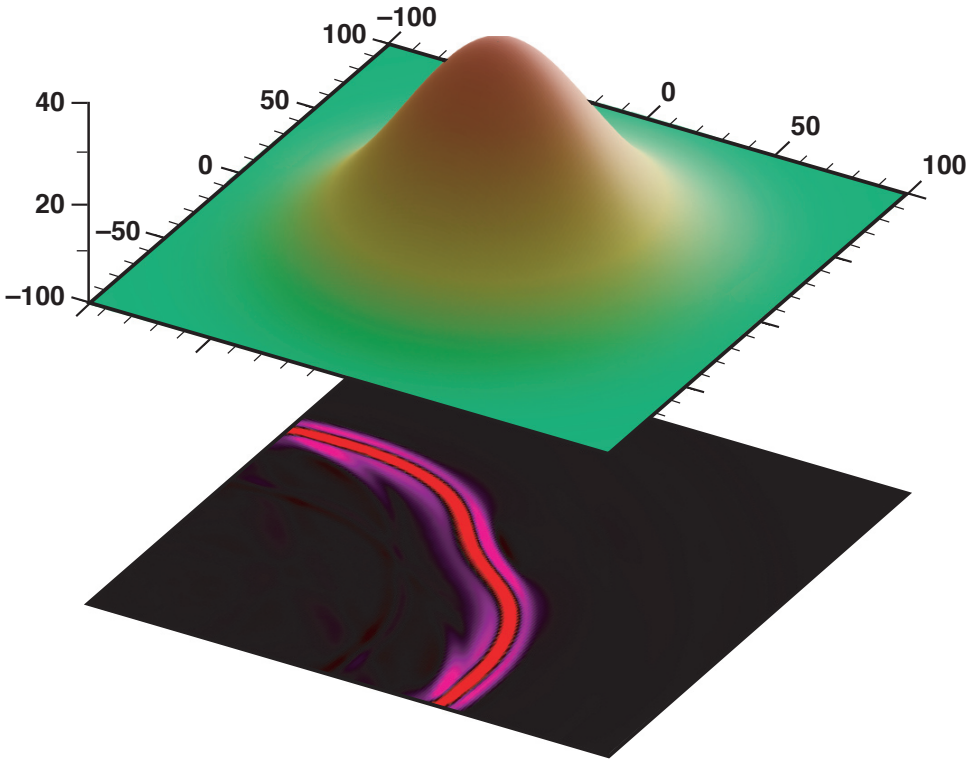

Figure 1. The wavefield for a simulation with the topographic feature is shown (purple for P-wave, red for S-wave). Without topography, the geometry of the wavefield would be a perfect semicircle.

Advances in wireless communication: LLNL technology base development efforts in self-configuring wireless communication of sensor data was augmented by direct investment of this project in a wireless module that would telemeter data from the Reftek Data Acquisition Systems in real time. The capability was necessary for any demonstration of real-time vehicle tracking. This capability was built but not in time for the tank tracking experiments, which were done on a proof-of-principle basis. The telemetry capability is being employed in the on-site vehicle tracking testbed now being completed. The wireless telemetry module is based on an IEEE 802.11b network card for wireless Ethernet communication. The major components of the module are shown in Figure 2 below along with the geophones used for some tracking applications.

Implementation of the K-L method: The Karhunen-Loeve (K-L) method (Van Trees, 1968) is a mathematical technique for building complex property distribution models that is particularly well suited for modeling the complex heterogeneity in earth materials and geologic structures. The method allows for the construction of basis functions, each with specific gradational transitions and covariance structures for each given property. A realization, or completed model, is created by summing the weighted basis functions. The method was adapted to the modeling of elastic wave speed distributions in two dimensions (2D). As shown in Figure 3, the basis functions (layered distributions on the left side of the figure) are weighted and summed to create the distribution on the right side of the figure. In two dimensions, specification of a small vertical correlation length and a large horizontal correlation length gives rise to earth-like stratigraphic layering of the property value. Methodology was also implemented that allowed for random variation of source property value, within basis function constraints, to create many random "realizations" of property distributions consistent with the basis functions and the statistical parameters of the property value.

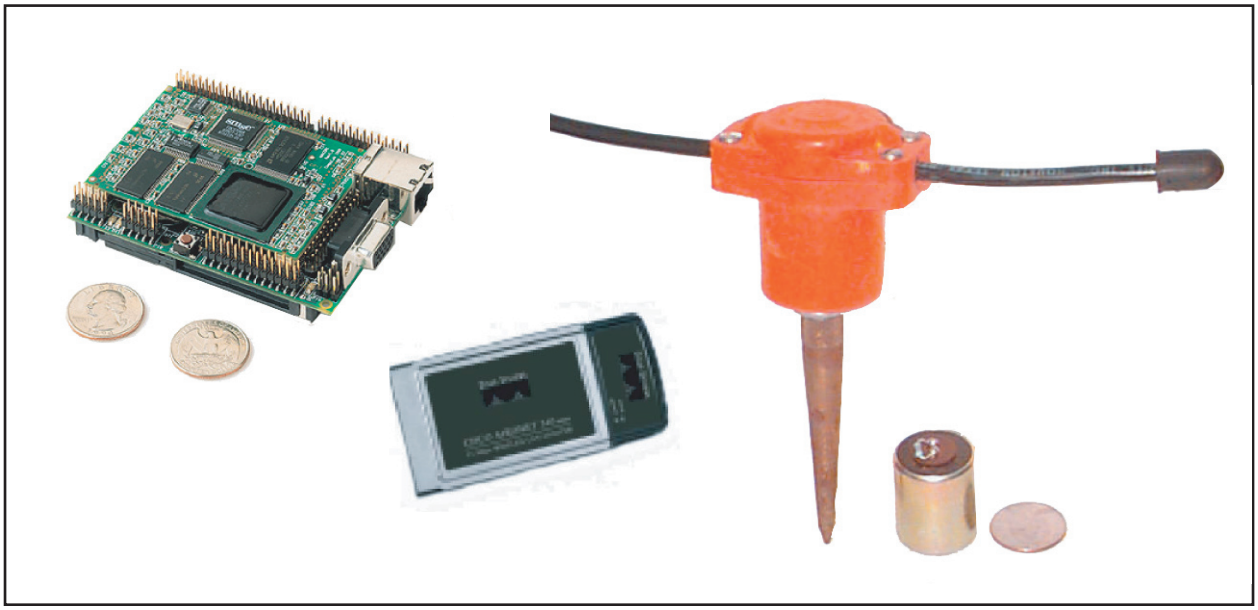

Figure 2. The single-board computer (left), the wireless ethernet card (center), and a typical geophone sensor (right) that form the basis of the acquisition and communication module.

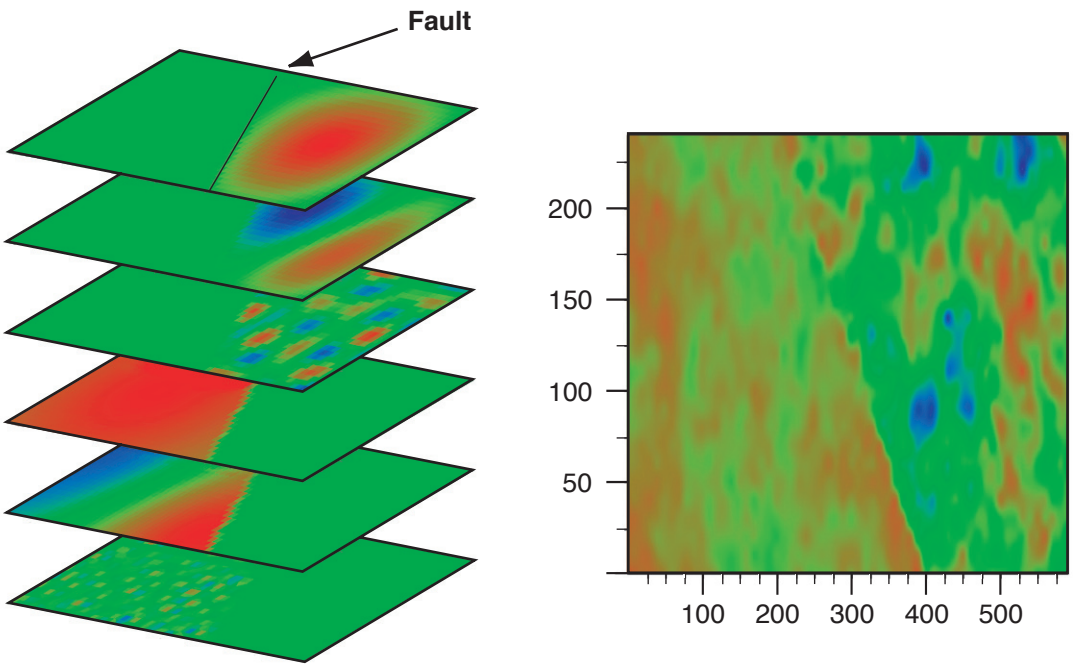

Figure 3. The left layers represent the variation of the given property consistent with statistical structure set up for that layer. The weighted sum of all layers produces the final property model shown on the right.

Vehicle Tracking

Matched field processing, the spatio-temporal generalization of matched filtering, operates in this application by correlating the set of matching wavefields (one for each potential source location) against the continuous (multichannel) data stream recorded by the distributed network of seismic arrays. In this application, matching wavefields may be developed from a simple (e.g., plane wave) model, computed from a more general model (E3D) or measured (calibrated).

In a strongly heterogeneous propagation medium, calibrated matching fields will provide much more accurate vehicle tracks at higher resolution than will a priori modeled fields. Indeed, calibration may be required for coherent combination of observations from several arrays.

Geological heterogeneity and the resulting wavefield complexity can, in the case of vehicle tracking, be effectively dealt with by direct measurement. In so doing, an operational assumption is made that a test vehicle calibration of the tracking area can be accomplished prior to actual tracking. This assumption will certainly not be valid in some scenarios and consequently a model-based approach to heterogeneity would be required in such cases. Since a model-based approach is unavoidable in tunnel detection applications, we chose to focus on a data-based calibration approach in vehicle tracking applications. We are using matched field processing (MFP) as our tracking/mapping paradigm because the matched field computations can be quickly accomplished on a modern PC even if the matching data set is very large. Consequently, in-field processing and assessment become possible and thereby open up a unique niche of seismic monitoring applications.

The fundamental approach is shown in Figure 4. As a vehicle drives through the tracking region,

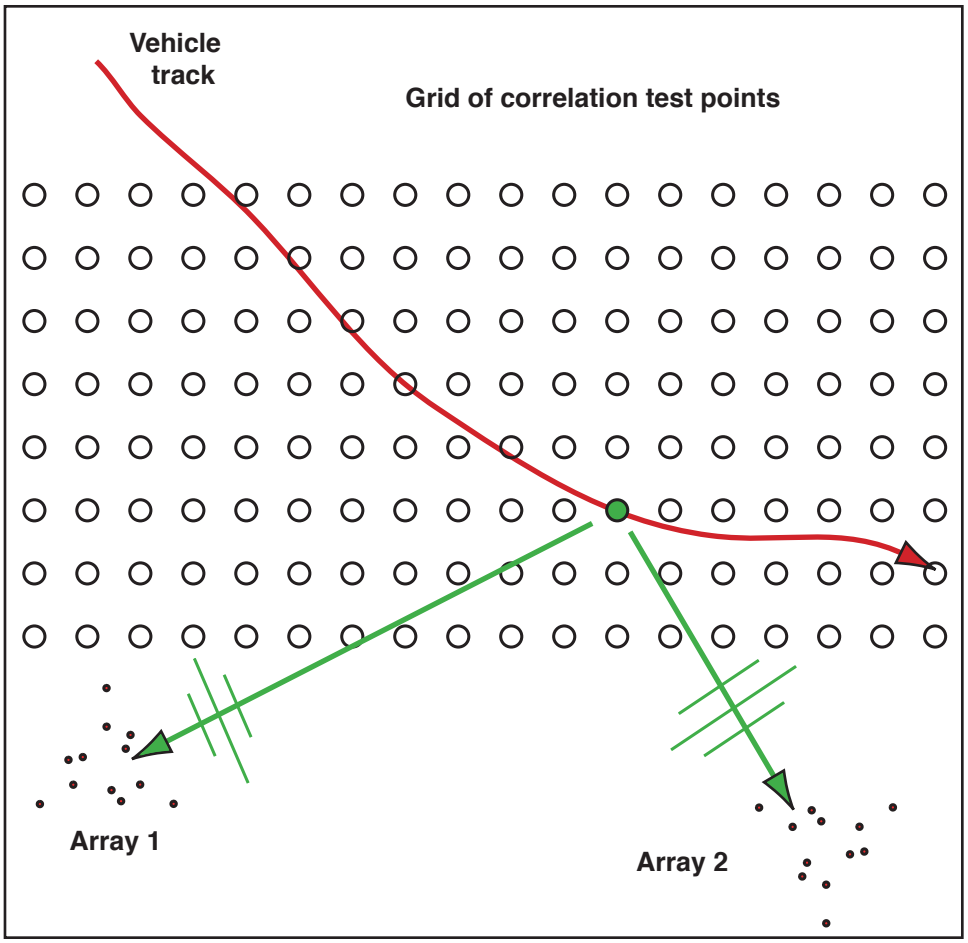

Figure 4. The matched field approach compares calibrated signal data associated with each grid point with the incoming data to find the best grid point match and hence the vehicle position at that instant.

seismic signals recorded from two arrays are compared with the "calibrated" signals obtained from a previous test vehicle and associated with each grid point. The grid point with the best matching field to the actual data is the best estimate of vehicle location at that instant. It should be noted that this processing approach is distinct from an FK (frequency-wavenumber) analysis from each array that gives a back-azimuth vector pointing to the location of the vehicle. With good angular separation of two arrays, the intersection of two back-azimuth vectors obtained from FK analyses of each array could also be used to track the vehicle position. Practice has shown that the FK system is not as accurate and becomes very unreliable if there is any significant seismic source outside the tracking region.

Tracking tanks in the desert: Vehicle tracking using seismic arrays and data-based matched field processing was tested at the Nevada Test Site on June 26–28, 2001. The generation of matching fields was accomplished by driving an M1A1 tank (see Figure 5), supplied by the state of Nevada Army National Guard, on a prescribed pattern that completely covered the tracking area, crossing every grid point. An on-board differential Global Positioning System (GPS) log provided the precise location of the tank at any specific time. The waveform recordings of each array in a short time window during which the tank was at a specific grid point location served as the "matched field" for a vehicle at that specific grid point. The matching process then corresponds to a cross-correlation of array data for a vehicle of unknown location within the tracking area with each grid point's "matching field." The best match corresponds to the vehicle location during the time window of analysis. Such a matching process is not computation intensive and can be accomplished by modern PCs in near-real time with some focused software development. In this experiment, we sought proof-of-principle, not a real-time tracking demonstration.

Two vertical-component short-period seismic arrays were deployed for the purpose of tracking and a separate fan-array for vehicle seismic signature characterization. The array apertures were on the order of 100 m and as far as two km away from the farthest part of the test region.

The M1A1 tank also served as the "unknown vehicle" or tracked vehicle (as opposed to the calibration vehicle use of the same tanks). It was driven on a scripted parallel row pattern as shown in Figure t3. The on-board GPS position log and the array recordings were later analyzed to determine actual vs predicted position. The data acquired and analyzed using matched field

Figure 5. M1A1 tanks supplied by the Nevada Army National Guard as vehicles for the tracking experiments.

processing successfully tracked the vehicle to an accuracy of 30 m at distances of a few kilometers as shown in Figure 6.

The experiment demonstrated proof-of-principle using calibrated or data-based matched fields to track a single vehicle. Simultaneous tracking of more than one vehicle should, in-principle, be possible but it was not attempted in this series of tests. In addition, near-real-time application of this tracking method can be accomplished, but it will require adapting the processing software and establishing direct communication of the real-time geophone data to the analysis computer.

Building 170 tracking testbed: Although the basic tracking approach was demonstrated in the tank tracking series of experiments, an attempt was made to integrate some of the technology developments mentioned earlier—in particular, wireless communication of the geophone signals—to create a wireless interface to a web-based real-time vehicle tracking prototype. The concept is as follows: three six-element seismic arrays monitor a specific roadway. The real-time geophone signals are transmitted to a central data acquisition and analysis platform that is web enabled. The images from an overview camera fixed on the test area also transmits images in real time to the same central platform. A user can then access the analyzed data via the web and see near-real-time images of the roadway along with matched field predictions of the position of vehicles on the roadway based on an analysis of the transmitted array data. The development of this prototype system should have basic functionality by the end of FY03. This project supported some of the initial efforts in FY02, but a different funding source supported FY03 efforts. The discussion that follows details the current project status based on FY02 and FY03 efforts.

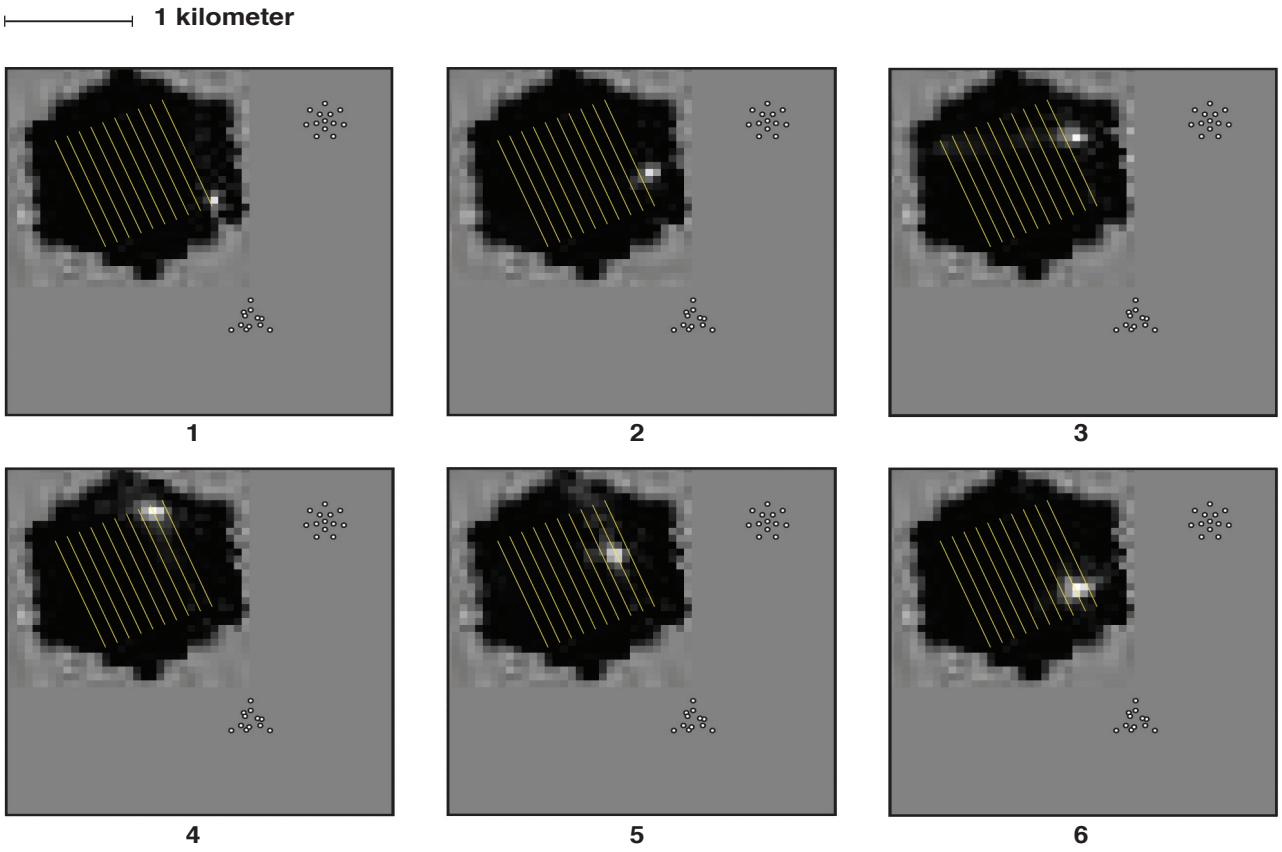

Figure 6. Matched field results showing snapshots of the array-determined location of the tank compared to the actual track lines the tank followed.

The roadway that was chosen is located within the LLNL site in the immediate vicinity of Building 170. Each seismic array consisted of six geophones hardwired to a central digitizing, archiving, and prototype telemetry unit (see Figure 7). Operating permissions from appropriate Laboratory offices were obtained for the array placement, the monitoring camera, the wireless telemetry, and the connection to the Open Lab Green Network. For early test and integration purposes, the wireless transmission was restricted to a single array and an FK analysis of the array data was to be displayed along with the camera images.

The central computer is located in a Building 132 office with a hardwire connection to the roof-mounted receiver antenna. The testbed status as of this writing is:

- Three seismic arrays installed.
- Central computer, receiver antenna, and camera installed.
- Wireless transmission, from one array of six geophones, functional.
- Web interface software written and ready for integration.
- FK analysis software written.

The remaining task is to port the FK analysis software to the central computer and configure for near-real-time processing in the integrated operational environment. After the wireless sensor testbed is functional, follow-on internal support will be sought to continue development and exploitation of this capability. We anticipate that other applications, far removed from vehicle tracking and seismic sensors, will want to utilize the real-time wireless communication interface to a web-based analysis and display tool that this testbed develops.

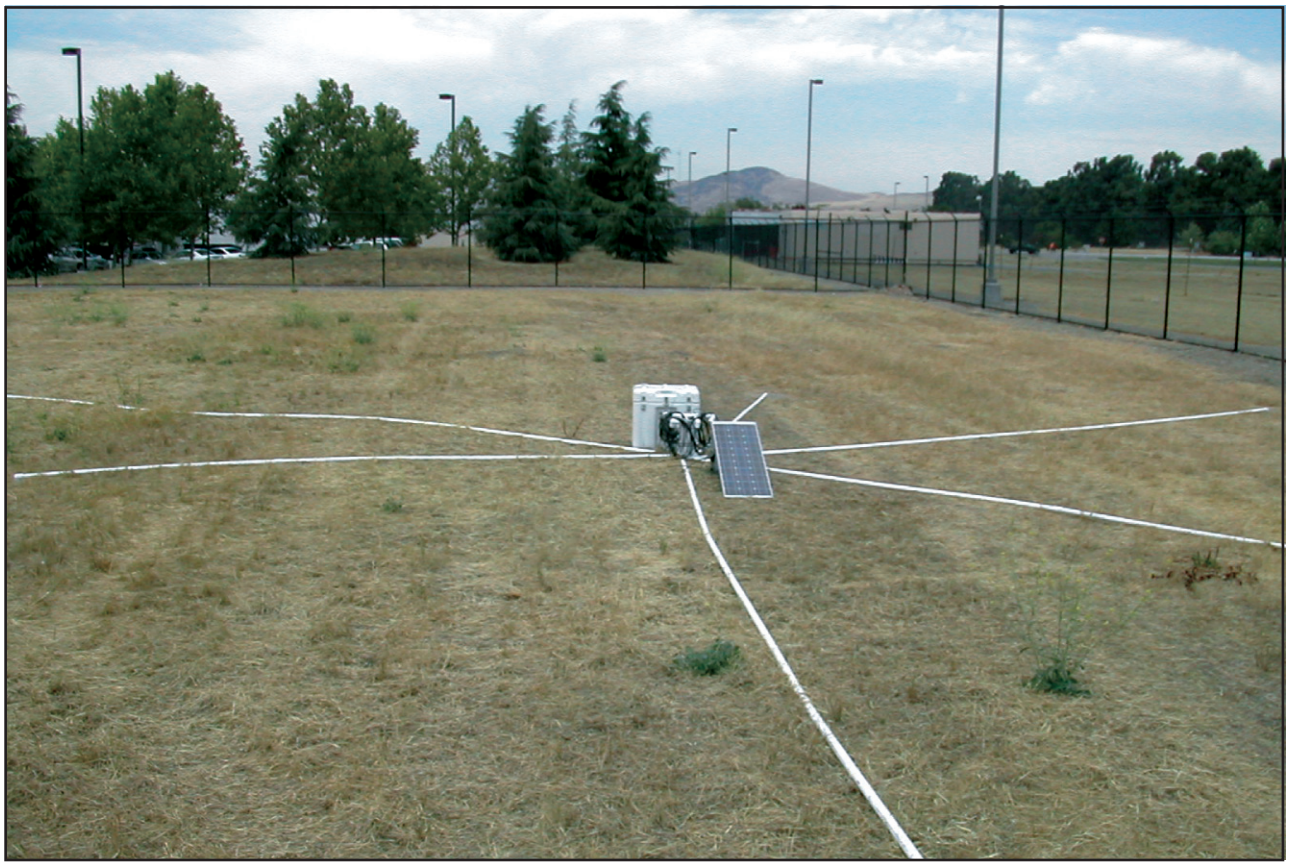

Figure 7. One of three six-element seismic arrays near Building 170. The white box is the digitizer/recorder and houses the prototype transmitter. The PVC piping protects the wires connecting the geophones to the digitizer from rodents.

Simulation Experiment

To determine if the overall processing strategy has merit and to identify any shortcomings in the analysis methods proposed, a simulation experiment was planned and conducted. The goal was to implement matched field processing (Fialkowski, 2000) on a set of realizations sampling the geological heterogeneity for a specified spatial correlation structure. To determine whether a tunnel can be reliably detected in the presence of geologic heterogeneity, seismic simulations were conducted for each realization with "tunnel-in" and "tunnel-out" configuration. We used the E2D code to carry out the 2D simulations. A key question for the geological heterogeneity strategy is: Will a representative suite of geological realizations improve reliability compared to a single base model?

The simulations were conducted as follows from a homogeneous base model:

1. **Generate realizations:** 200 geological realizations about the base model were computed using the K-L methodology.
2. **Form pairs:** A tunnel-in and tunnel-out version of each of the 200 geological realizations was produced.
3. **Compute wavefields:** The full wavefield for each of the realization cases was computed (400 total).
4. **Determine matching set:** A matched field set was formed for specific source and receiver locations using 1, 2, and 5 realizations from a reserved set of 50.
5. **Matched field processing:** 300 wavefields (each a tunnel-in and tunnel-out pair from 150 geological realizations) were "matched" against the matched field set.
6. **Statistical analysis:** Statistical curves [Receiver Operator Curves (ROC)] were produced for each matched set (1, 2, and 5) to summarize the tunnel-in vs tunnel-out discrimination results.

Generate realizations: The procedure used to generate the realizations is based on the K-L methodology, which assigns random changes to a specific property value with position according to the specified probability distribution and feature correlation. The methodology as applied here allows the specification of a horizontal and a vertical correlation length. In this series of simulations we used a vertical correlation length of 15 m and a horizontal correlation length of 1000 m. The vertical correlation length was deemed a typical lithologic thickness from many of the potential application sites we could envision. The horizontal correlation length of 1000 m was chosen to emulate horizontal bedding that is consistent with and typical of a sedimentary depositional environment. The P-wave heterogeneity mean was fixed at 10% of the base model value. Figure 8, left figures, shows two geological realizations produced using this methodology. Note the similarity to typical horizontal geological bedding with ex-tended pinching of non-continuous horizontal lenses, a direct result of the correlation lengths chosen.

Form pairs: For each geological realization, a tunnel-in and a tunnel-out version are produced. The tunnel-out version is the realization model. The tunnel-in version is made by changing the P-wave speed and elastic properties of the model in the tunnel region, as shown by the white box within the realizations of Figure 8. The tunnel region is in the same location for all 200 geological realizations.

Compute wavefields: Using the E2D code, wavefields are calculated for each tunnel configuration (in or out) of each realization and for each shot location. In this simulation experiment there were two surface shot locations used making each realization have four associated wavefields: tunnel-in, shot 1; tunnel-

out, shot 1; tunnel-in, shot 2; tunnel-out, shot 2. The computed wavefields can be seen in the right figures of Figure 8.

Determine matching set: The matched field set required a significant degree of trial-and-error processing before a final set was fixed. An important consideration was to avoid confounding the tunnel-reflected body wave signal with the direct-path surface wave, the same concern as the NTS tunnel experiment. Although schemes for canceling the surface wave were explored, we ultimately decided to avoid this by choosing a source–receiver location that had a substantial arrival time difference between the direct surface wave and the tunnel-reflected body wave. Figure 9 illustrates the difficulties. Above the geological realization shown, the "S" is the surface source location and the "r" marks all the receiver locations. The waveform traces below are the E2D computed seismograms for each receiver: the top trace for the receiver location nearest the source, the second trace down for the second receiver from the source, and so on. The seismograms from each receiver are separated into two overplotted components: the direct surface and body wave signals (black) and the tunnel-reflected body wave signal (red). The figure clearly shows the source–receiver geometries that result in confounded arrival times, where the large surface wave phase and the tunnel-reflected signal are time coincident. The figure also clearly shows the geometries that are most favorable for separating the two arrival times: a close source–receiver spacing offset from the tunnel (top few traces). This geometry allows the direct surface wave to be long past the receiver before the tunnel-reflected signal arrives.

Figure 10 compares a geometry with sources (•) and multiple receivers (r) on either side of the tunnel (left plate) and the resulting surface wave and tunnel-reflected signal (below) with a source–receiver geometry that straddles the tunnel (right plate). As in the previous figure, the source–receiver geometries that are close in

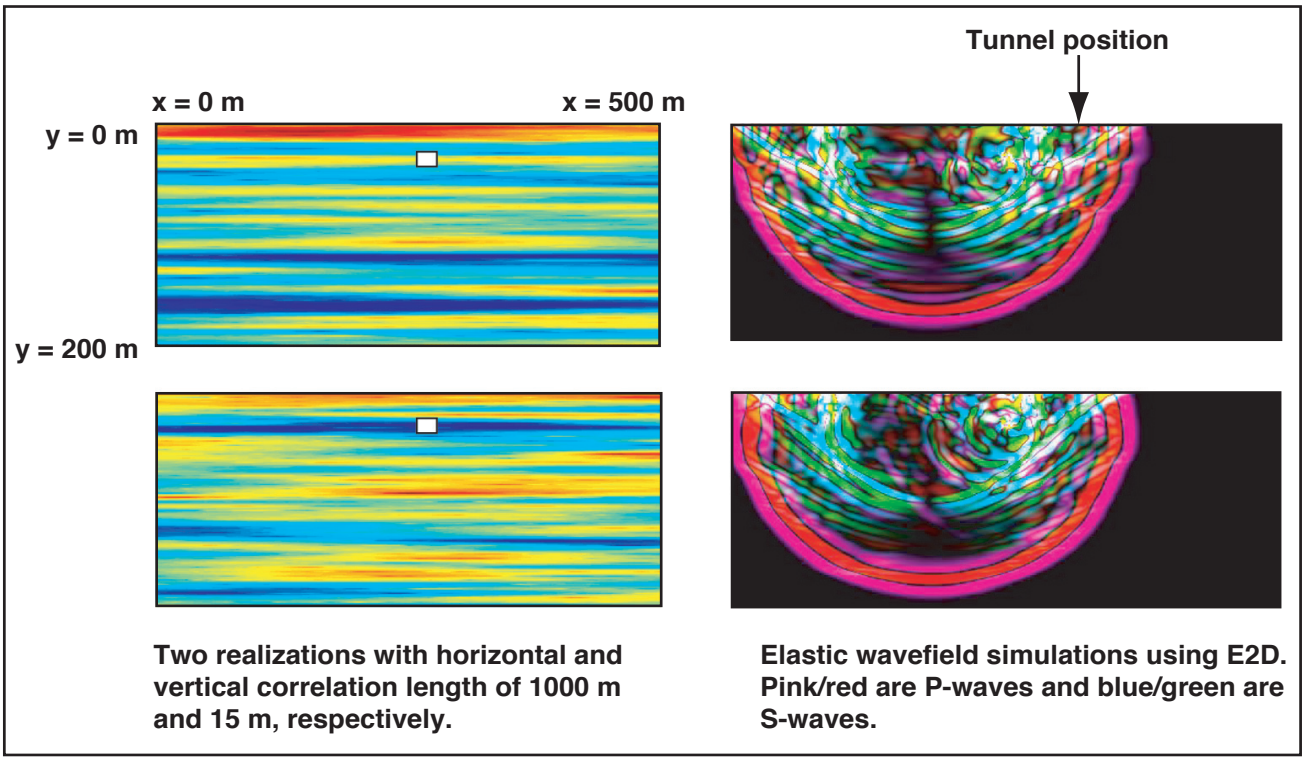

Figure 8. The corresponding E2D simulations (right) are shown for two geological realizations (left) for a tunnel located as shown by the white rectangle. Note the qualitative difference in the tunnel scattered signal between the two realization simulations.

spacing and that are offset from the tunnel provide the best arrival time separation. The left plate geometry was used in the simulation.The twelve receiver seismograms from the two sources in the tunnel-reflected signal arrival time analysis window were the match traces used in all analyses.

Matched field processing: The mock data set is the 150 tunnel-in/ tunnel-out wavefield realization pairs. Each of the 300 cases is matched against the reserved set of tunnel-in realizations. Although 50 tunnel-in realizations were reserved for spanning geological heterogeneity, only a small number were actually used. The effect of geological heterogeneity on the waveform features of the tunnel–reflected signal is shown in Figure 11. Ten geological realizations are shown and, for the source–receiver geometry shown, the tunnel reflected signal is computed by E2D for each realization. The waveforms have had all but the tunnel-reflected signal removed. The figure dramatically illustrates the complexity of the tunnel-reflected signal as well as the high variability of the waveform features when geological heterogeneity is applied. It strongly suggests the need to somehow account for or span the effects of geological heterogeneity on signal features. In this simulation experiment three cases were run: a single tunnel-in realization as

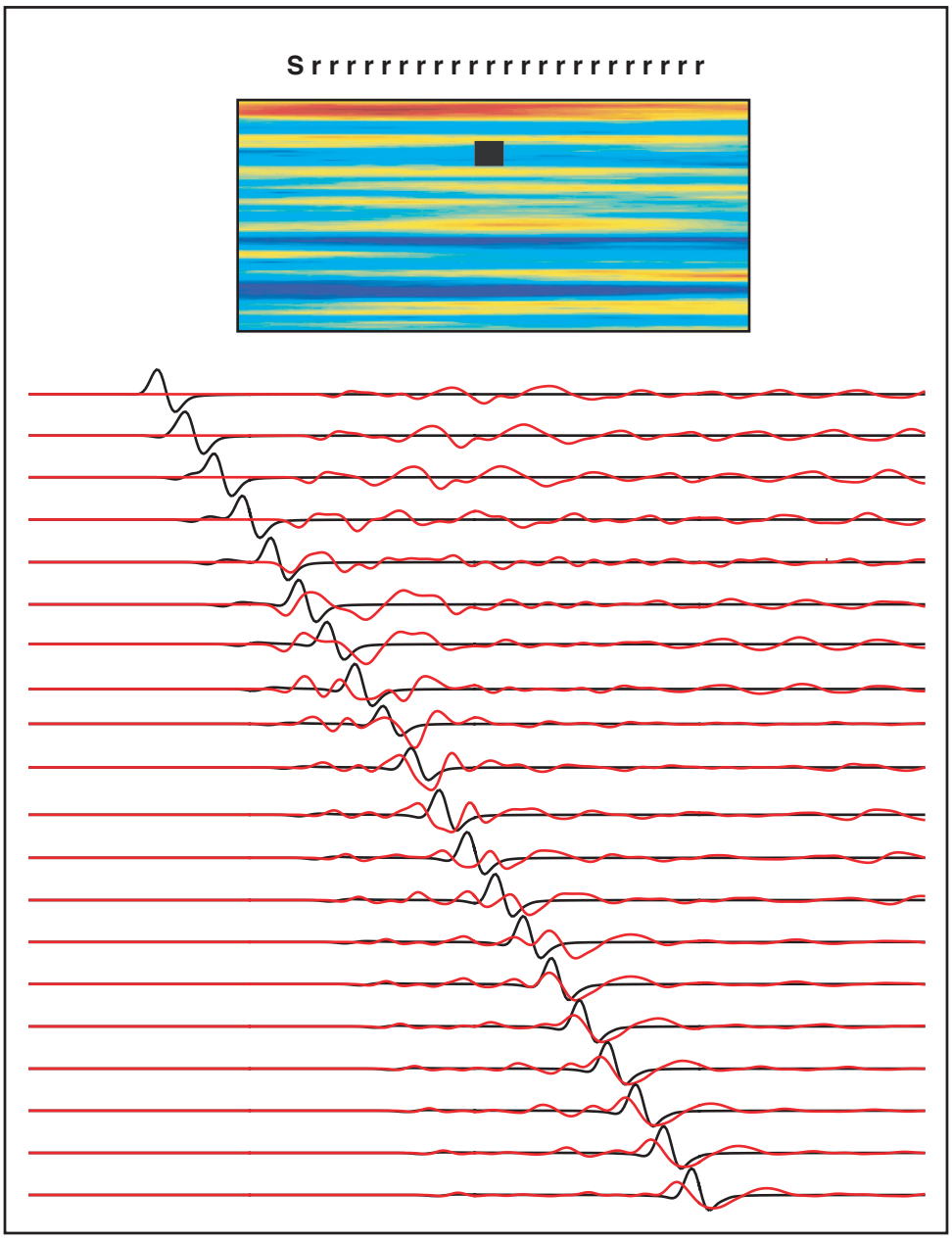

Figure 9. A geological realization (top) is shown with a single source, S, and receiver locations, r. The E2D simulated waveforms for each source–receiver pair are shown from smallest separation (top) to largest separation (bottom) for the tunnel-in simulation (red) and the tunnel-out simulation (black). Note the tunnel-reflected signal can best be distinguished from the large surface wave phase when the source–receiver separation is picked to keep the phase arrivals noncoincident.

the matching field, 2 tunnel-in realizations, and 5 tunnel-in realizations. The matched field processing scheme ultimately compares the selected receiver waveforms from the reserved set with the same selected receiver waveforms from each mock data wavefield realization. The full process is shown in Figure 12. The 200 geological realizations are used to produce 400 E2D calculated wavefields, each geological realization resulting in a tunnel-in wavefield and a tunnel-out wavefield. Selected receiver locations are used in the matched field processing as discussed earlier. The wavefields reserved for spanning geological heterogeneity are matched or cross-correlated against the mock data or the measurement test set. The result is a set of 300 numbers, two for each of the realizations (tunnel-in and tunnel-out).

Statistical analysis: The result of a single "matching" calculation is a number representing the goodness-of-fit of the mock data to the simulations spanning geological heterogeneity. The mock data is each of the 300 wavefield simulations (150 tunnel-out and 150 tunnel-in). The statistics of these goodness-of-fit numbers were analyzed in terms of probabilities of false alarms vs probabilities of missed detection. By choosing a given detection threshold, the 300 number analysis result set can be scored to determine how many tunnel-out values fall below and above the detection threshold. The same scoring is applied to the tunnel-in values of the mock data set. The number of tunnel-out realizations that have matching values above the detection threshold defines the false alarm probability. The number of tunnel-in matching values that fall below the detection threshold defines the missed detection probability. As the detection threshold value is varied from the lowest matching value to the highest matching value and probabilities are calculated for each incremental change in the threshold value, a curve is produced that defines the trade-off of

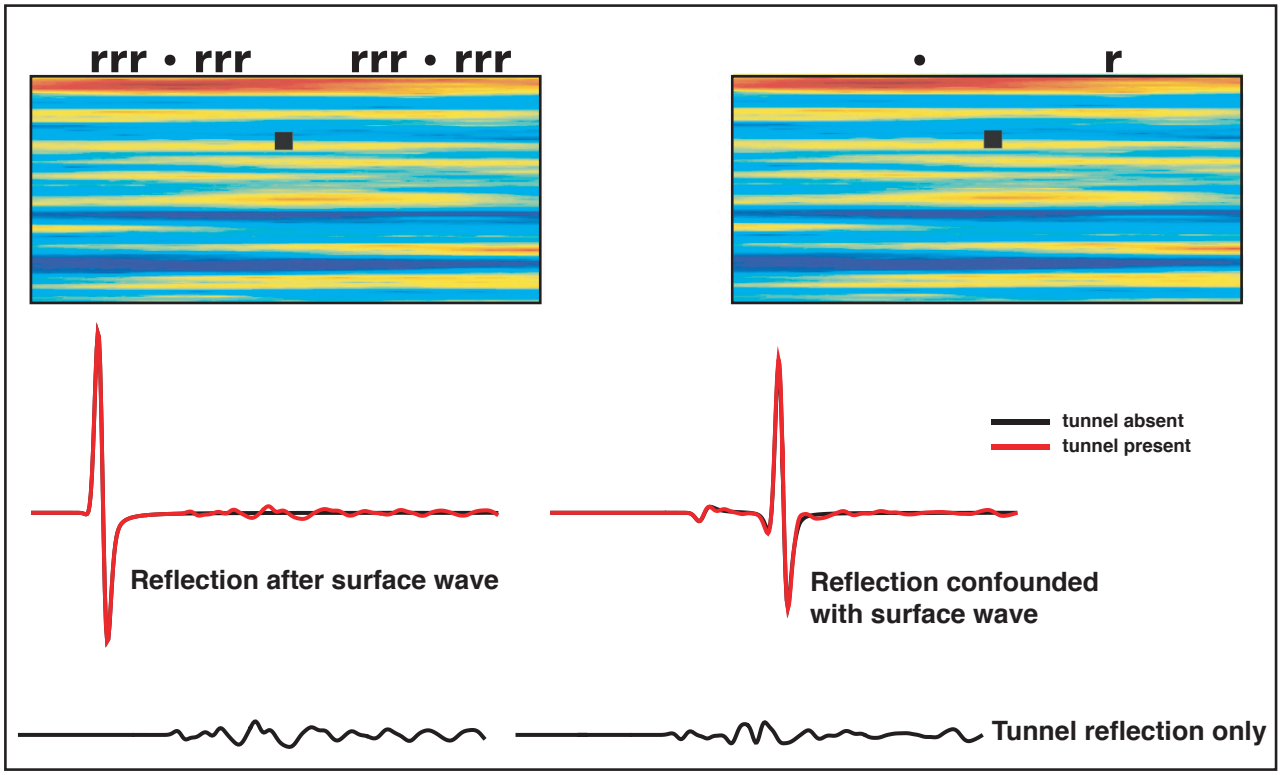

Figure 10. Two geological realizations are shown with waveform simulations below each corresponding to the source (•) and receiver (r) geometries shown for tunnel-in (black) and tunnel-out (red) simulations. Note that in the left simulation the tunnel-reflected signal arrives well after the large surface wave phase while the right simulation confounds the surface phase and tunnel-reflected signal.

false alarms vs probability of missed detections. This curve essentially quantifies the capability of the analysis methodology to distinguish between tunnel-in and tunnel-out configurations. An analysis was done for each of the three heterogeneity-sampling cases (1, 2, and 5 model samples). The result is shown in Figure 13. Clearly even using a single base model provides a good separation of the tunnel-in and tunnel-out populations. The blowup plot of Figure 13 reveals that the red curve (2-model spanning) is mostly left of the black curve and consequently is an improvement in the tunnel-in and tunnel-out population separations. The green curve, representing the 5-model spanning case, is not visible in the plots because it exactly overplots on the X and Y axes of the plots, representing perfect tunnel-in vs tunnel-out population separation results.

Although only five realizations were required to completely separate the tunnel-in and tunnel-out wavefields, we expect that the real world will show more complexity and variability and hence require a much larger suite of geological realizations. The main point here is that a randomly selected set of geological realizations can effectively span the set of geologic realizations, and this approach can improve the bottom-line result of detecting underground

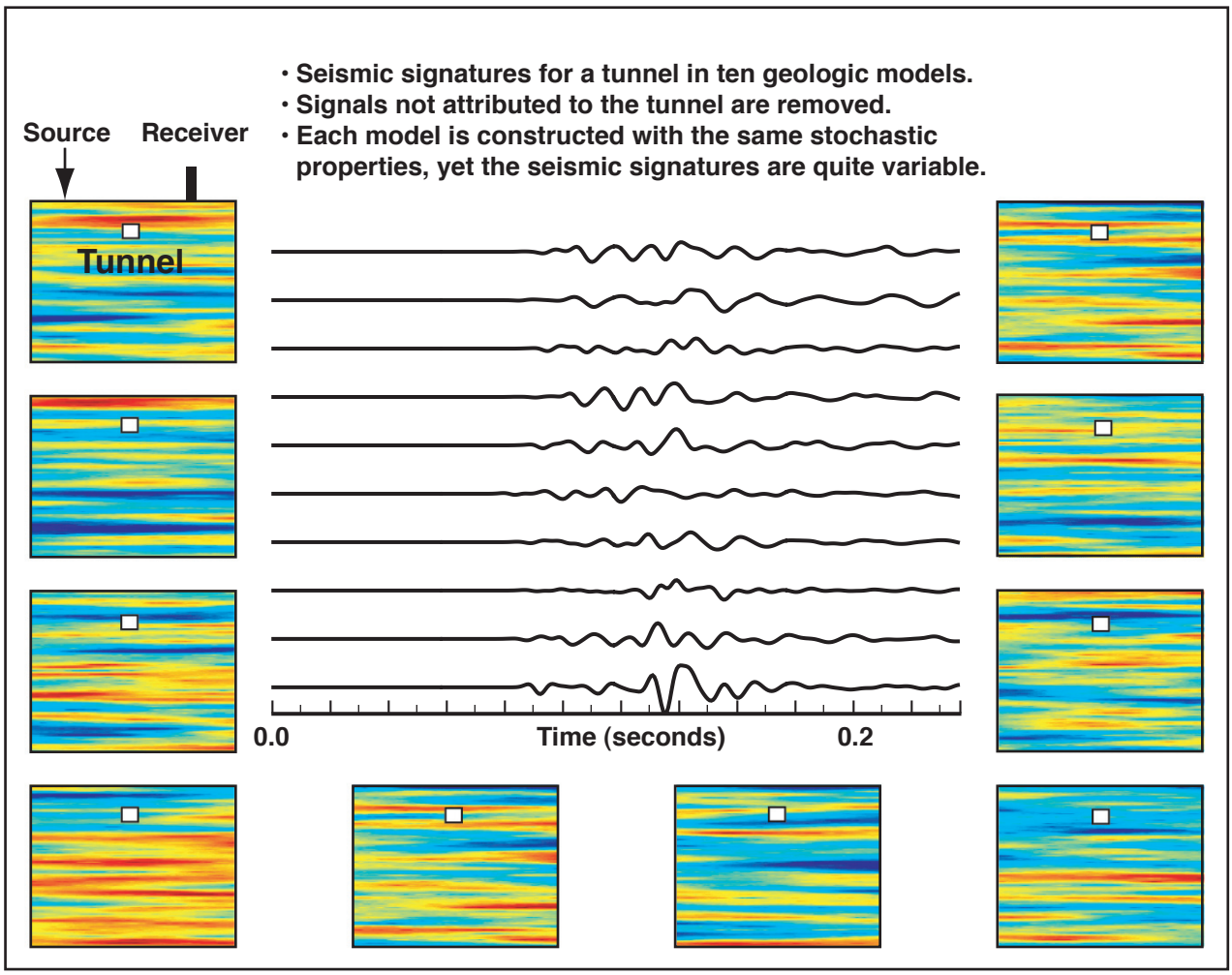

Figure 11. Ten geological realizations are shown surrounding the tunnel-reflected signals from each. The tunnel-reflected signals are produced by differencing the tunnel-in and tunnel-out waveform simulations. Note the great variation in the waveform features due to the geological heterogeneity between simulations.

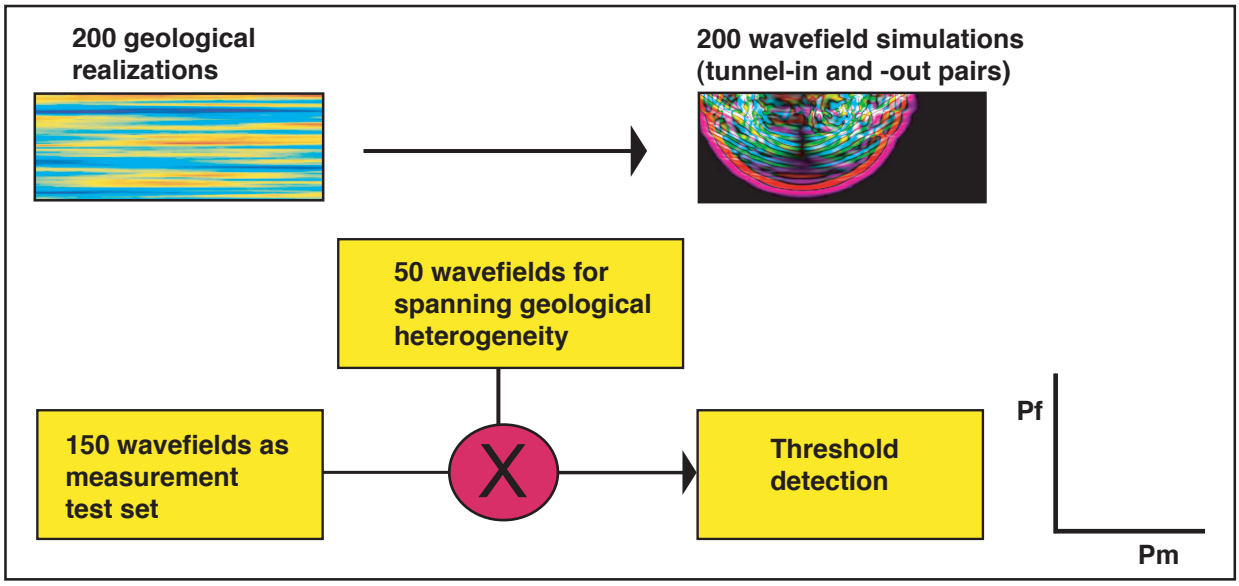

Figure 12. This summarizes the full processing methodology. Two hundred geological realizations produce a set of four hundred simulations (tunnel-in and tunnel-out pairs). Fifty pairs are reserved for spanning geological heterogeneity and 150 pairs constitute the measurement set. The "X" operation symbolizes the matched field processing of the measurement against the reserved set to produce goodness-of-fit numbers that a threshold detection are applied to. The final result is a curve depicting the probability of missed detections against the probability of false alarms.

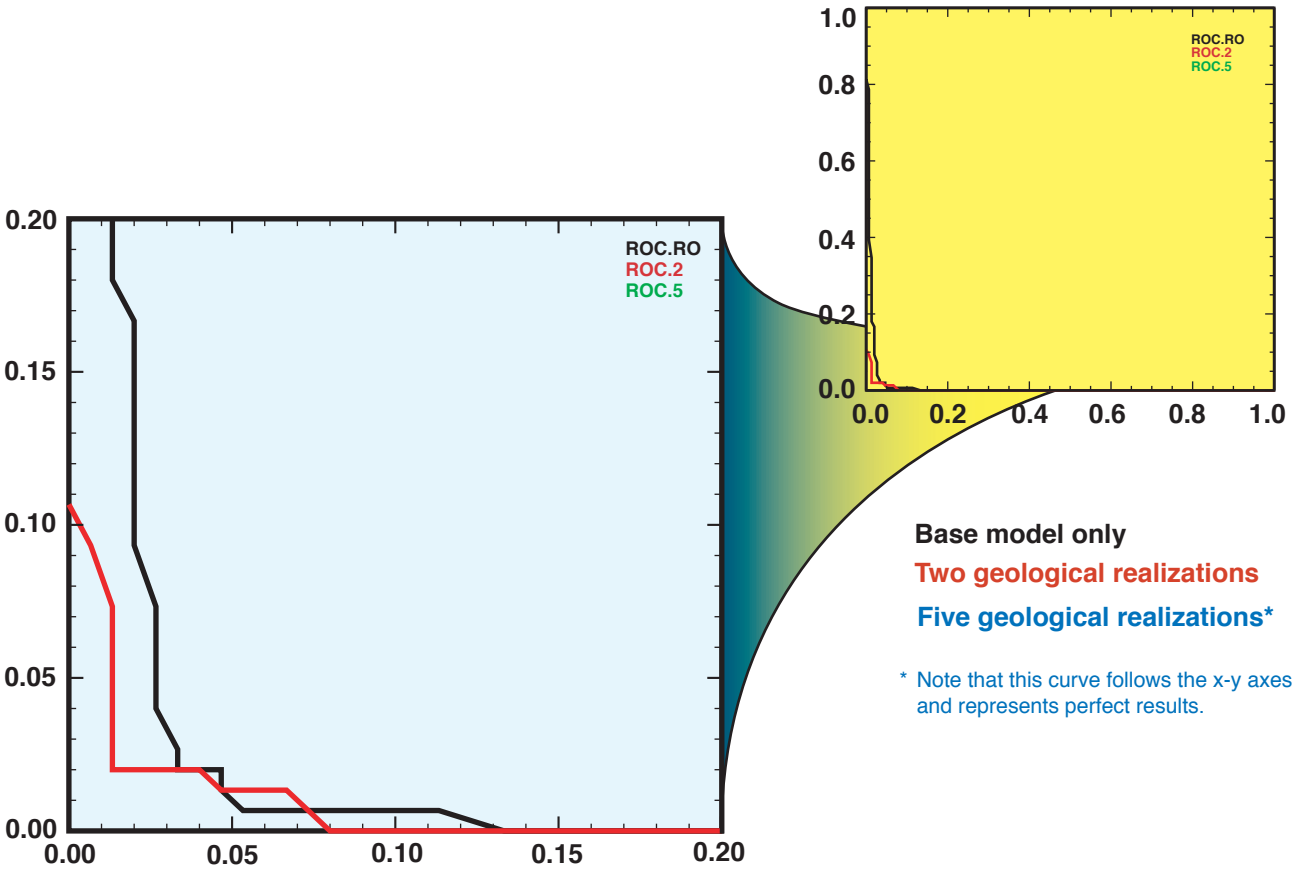

Figure 13. The ROC curve and blowup show the probability of missed detections against the probability of false alarms for the base model (black), spanning with two realizations (red), and spanning with five realizations (green). Note that more realizations improve the classification statistics and that five realizations result in perfect population separation (green not visible because it plots along the X-Y axis).

Nevada Experiment

An experiment was conducted in December 2001 at the Nevada Test Site (NTS) to determine if a reflection signal off a tunnel could be observed and ultimately utilized in matched field processing analysis. The deployment was in preparation for a much larger experiment. The specific goals were to determine if surface waves would confound the interpretation of the body wave tunnel-reflected signal and to assess the variability of the reflected signal waveform.

The site used was a shallow tunnel as shown in Figure 14. The shallow depth of the tunnel allowed us to employ a simple hammer source. Geophones were mounted on the ground surface above the axis of the tunnel. An initial series of hammer blow calibration recordings were used to characterize the medium velocity, signal characteristics, and help plan the scale and spacing of the geophones and source locations.

The sensor spacing was chosen to be small enough to preserve coherency for the highest frequencies recorded in the initial calibration tests (2 m). The surface wave was expected (based on simulations discussed below) to be the largest amplitude signal and since it travels at a slower speed than the P and S body waves, as the source is moved farther away from the geophones, a point is reached where the faster body waves reflected off the tunnel will arrive before the direct-path surface waves despite the longer travel path (about 30 m). Source locations were chosen to adequately sample well short of and well behind this expected phase arrival crossover point (see Figure 15).

The experiment was simulated using E2D to calculate the synthetic seismic records. Although the synthetics were eventually compared to actual field data, their first use was to help define the scale and layout of the field experiment. The simulation used a constant velocity medium that matched the experimentally determined material velocity. E2D also simulated the same experiment without a tunnel present. This was

Figure 14. Photograph looking down the axis of the test site tunnel.

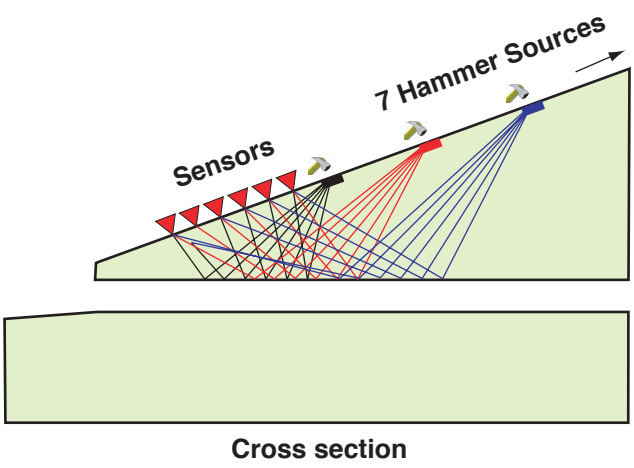

Figure 15. Cross-section view of the experiment layout above and along the axis of the tunnel. Sensor spacing is 2 m, source spacing is 10 m.

used to help identify the tunnel-reflected signal in the presence of direct wave phases. The simulation is shown in Figure 16. The tunnel-reflected arrival was determined by comparing with an identical simulation run with the tunnel absent. The simulation shows that for source–receiver distances of less than 30 m (right plot and bottom of center plot) the tunnel arrival is confounded with the surface wave (the largest amplitude signal that correlates across the waveform traces). That is to say, their arrival times overlap, and consequently it is very difficult to determine a priori the presence of a tunnel-reflected signal riding on a large amplitude surface wave signal. For source–receiver distances greater than 30 m (left plot and most of middle plot), the tunnel-reflected signal arrives before the direct surface wave arrives (because of its slower speed) and can be easily discerned. These results were crucial in defining the sensor and source layout so that records were taken with adequate source–receiver distance to assure an arrival time separation in tunnel-reflected signal and surface wave arrival times.

Comparison of the simulated waveforms with actual data is shown in Figure 17. This figure shows the simulations with and without a tunnel present (bottom plots) compared to recorded data (top plot). Recorded data and simulation with a tunnel show fairly good qualitative correlation, suggesting phase arrival time of the tunnel-reflected signal in the recorded data.

The conclusions drawn from this preliminary experiment are:

1. For this simple geometry, the simulations reflect the complexities observed (in both timing and waveform shape) and are crucial in defining the tunnel-reflected signal in the recorded data.
2. Simulations are useful in planning the experiment, particularly in understanding the source–receiver geometry that will separate surface wave and tunnel-reflected phase arrival times.
3. For the shallow tunnel depths of this experiment, strong tunnel-reflected signals are observed in the recorded data.

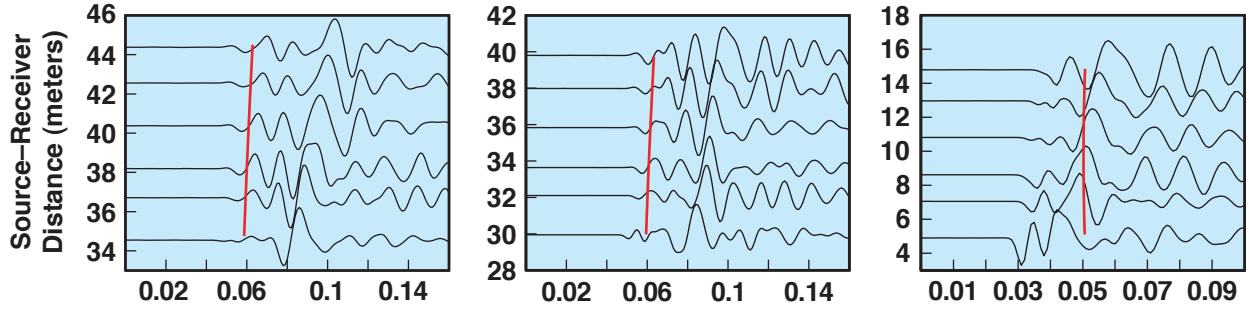

Figure 16. Simulated recordings using three different source locations. The red line defines first-break of the tunnel-reflected signal arrival.

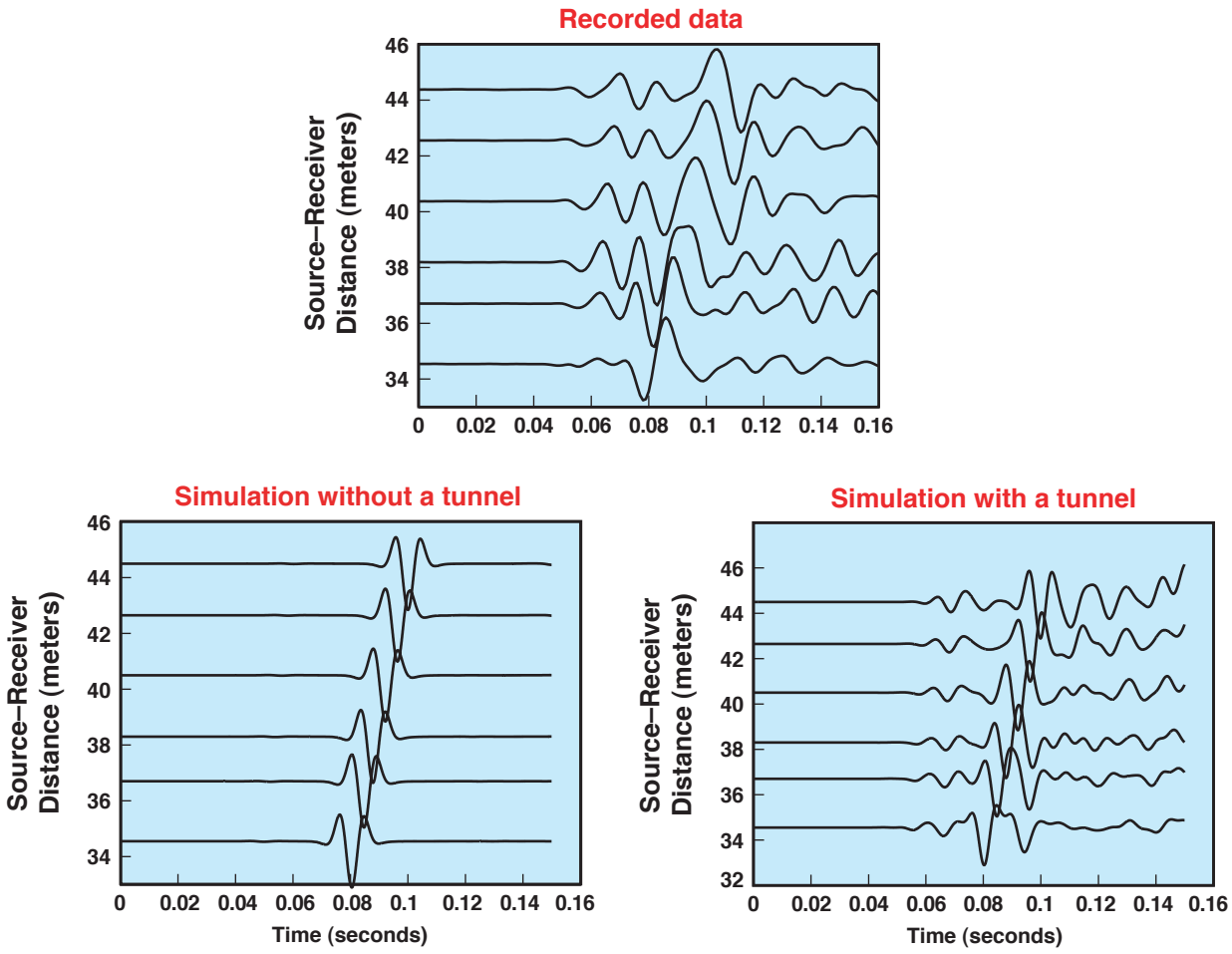

Figure 17. Comparison of field data to simulation with and without tunnel present.

Lake Lynn Experiment

A change in the NTS site use schedule meant that the planned follow-on experiment to the NTS tunnel deployment could not be conducted during the time frame of this project. An alternative site was located at the Pennsylvania/West Virginia border. The site is called the Lake Lynn Laboratory, an old pillar-room mine extensively developed as an experimental mine safety facility. Routine controlled mine explosions and fires are conducted to study various safety issues. The Lake Lynn Laboratory is a part of the Pittsburgh Research Laboratory within the National Institute for Occupational Safety and Health (NIOSH), all part of the Centers for Disease Control and Prevention.

The objective of this experiment was to conduct the full tunnel detection experiment on a realistic facility to test the full application of the analysis methodology. The Lake Lynn site had a number of features that would make it particularly challenging to both conduct an experiment and model the site. It had the distinct advantage of being available to us with excellent NIOSH support in logistics and in conducting explosive shots. The Lake Lynn site is located in hilly terrain with tunnel depths generally deeper than can be detected with reflection seismology. A survey of the area did reveal a small area of shallower tunnel depths on a scale appropriate for our experiment. The area was complicated by the presence of a vertical wall (the "highwall") and

Figure 18. Photo of the central tunnel, the highwall, and the hill above it from the central survey reference point. Note the white data acquisition system boxes scattered on the hillside that give a rough indication of the location of the geophones.

a steep hillside upon which sensors and shots would have to be emplaced. Figure 18 shows the experimental site area and the highwall.

The layout of the field sensors was based on the use of small six-element arrays spread along the primary tunnel axis and perpendicular to the tunnel axis with a second line parallel to the tunnel axis but offset from it. Due to a narrow time slot to conduct the experiment, the complexity of the modeling, and the inherent 3D nature of the problem, we could not develop E3D model runs in advance of the deployment to guide us on optimizing layout to separate surface wave arrivals and tunnel-reflected signal arrivals. Instead, simple calculations coupled with numerous sensor locations and shot locations were employed to be sure that the appropriate data would ultimately be acquired.

The test site was chosen to be over an area containing the shallowest obtainable tunnel depths and such that a simple tunnel vs nontunnel analysis could reasonably be accomplished. This was difficult and was ultimately a compromise given the terrain and the complexity of the mine. Figure 19 shows the site area elevation contours and mined footprint overlain on a satellite photo of the region. Our test site is within the superimposed rectangle, surrounding the rightmost tunnel perpendicular to the highwall that leads to the old room-pillar mine workings. By working as close to the highwall as possible, we attempted to isolate and focus reflection studies on the single tunnel at shallowest depth.

The surveyed data and AutoCAD Drawing file supplied by NIOSH was used to construct a topographic model using supplied contour lines, building locations, and other data. A triangulated irregular network (TIN) was created

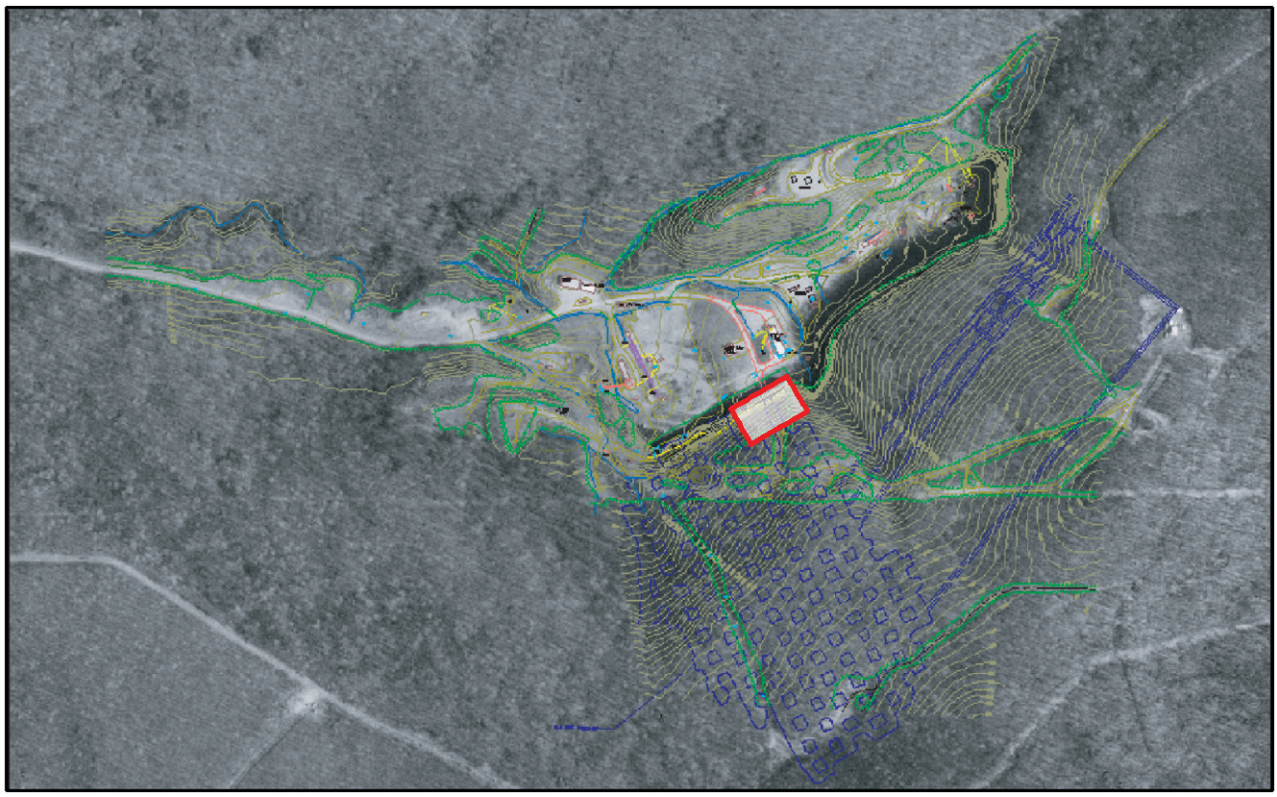

Figure 19. An aerial overview of the Lake Lynn site with contours and the mine workings footprint (in blue) overlaid. The complete test region is within the red rectangle shown.

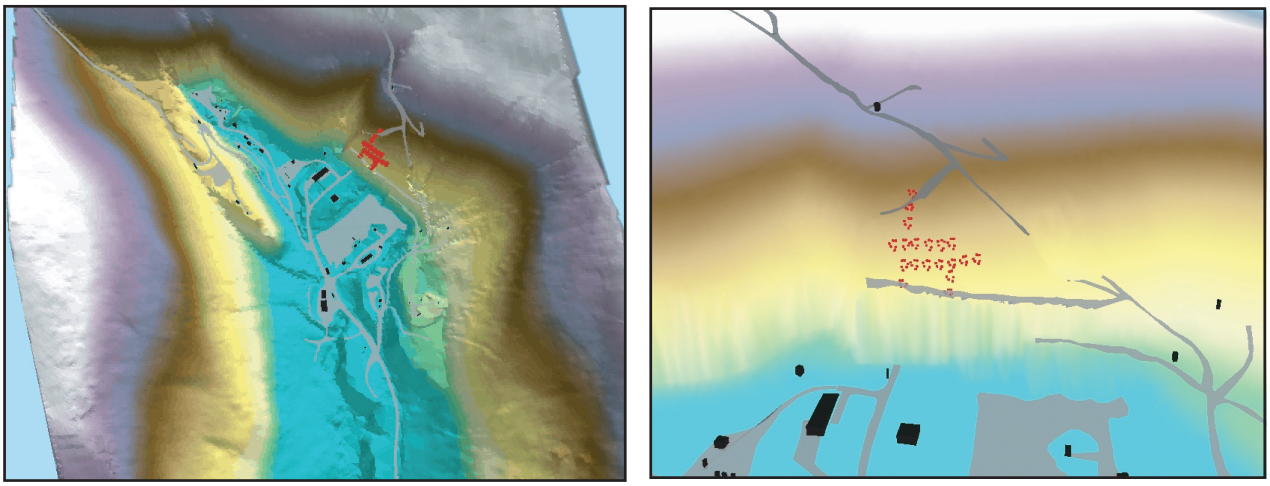

Figure 20. The TIN models of the topography and sensor layout at Lake Lynn. The right panel is a blowup of the left one centered on the sensors.

using the program ArcScene. Other features were projected onto the TIN to create the model shown in Figure 20 at two scales. Note the layout of the sensor arrays; two lines paralleling the tunnel (one above it and one over competent formation) and two lines running perpendicular to the highwall, one upslope from the other.

The array aperture chosen was 6 m to adequately preserve coherence over the signal frequencies we expected (up to 150 Hz) and the array geometry was that of a six-element Golay array as shown in Figure 21. An effective method for rapid deployment of consistent array geometry was employed that used two fixed 2-m equilateral triangle frames (see Figure 21). By compass aligning the "fixed" triangle frame, the moving triangle frame could be aligned to the fixed frame in such a way that the vertex points of the moving frame specified the proper

Figure 21. The photo shows the rigid 2-m triangles used to quickly lay out an array. To the right of photo is the geometry of the six-sensor Golay array.

sensor locations. Using this method, a six-element array could be physically emplaced in 5 to 10 minutes, even in rugged terrain. This does not include the time required to physically move a 70-lb data acquisition system (DAS) recorder and a 50-lb battery to the center of the array on the steep hillside. After the layout, all sensor locations and shot locations were surveyed to an accuracy of 1 cm. The surveyed locations showed that the rapid layout method provided a consistent geometry to sufficient accuracy.

Two types of shots were conducted during this experiment. The primary shots were shallow-buried 40-gm explosions to serve as the surface sources for measuring the tunnel-reflected signal. The second type of shot was a tunnel shot, used to investigate a special issue of interest to potential sponsors and related to the main focus of the experiment that will be discussed below. The tunnel shots were larger (500 gm) untamped shots within the tunnel complex. Figure 22 shows the shooting material and a typical seismic shot just fired. In all, 24 surface shots and 4 tunnel shots were fired. The total number of surface shots included many repeated shots and a few shots with 20 gm and 80 gm of explosive.

The sensors used were common seismic exploration grade 4.5-Hz free-period geophones without damping resistors. We used a total of 114 sensors configured in 19 six-element arrays on the layout shown in Figure 21. The six elements of each array were recorded by a single six-channel digital recorder. Two types of DAS were used, Reftek 16- and 24-bit models (14 units) and Geotech 24-bit recorders (5 units). Sampling rates were 500 Hz for all testing. Accurate timing was kept using GPS but this limited the inter-DAS timing accuracy to about a millisecond. The timing skew between channels within any data acquisition unit was

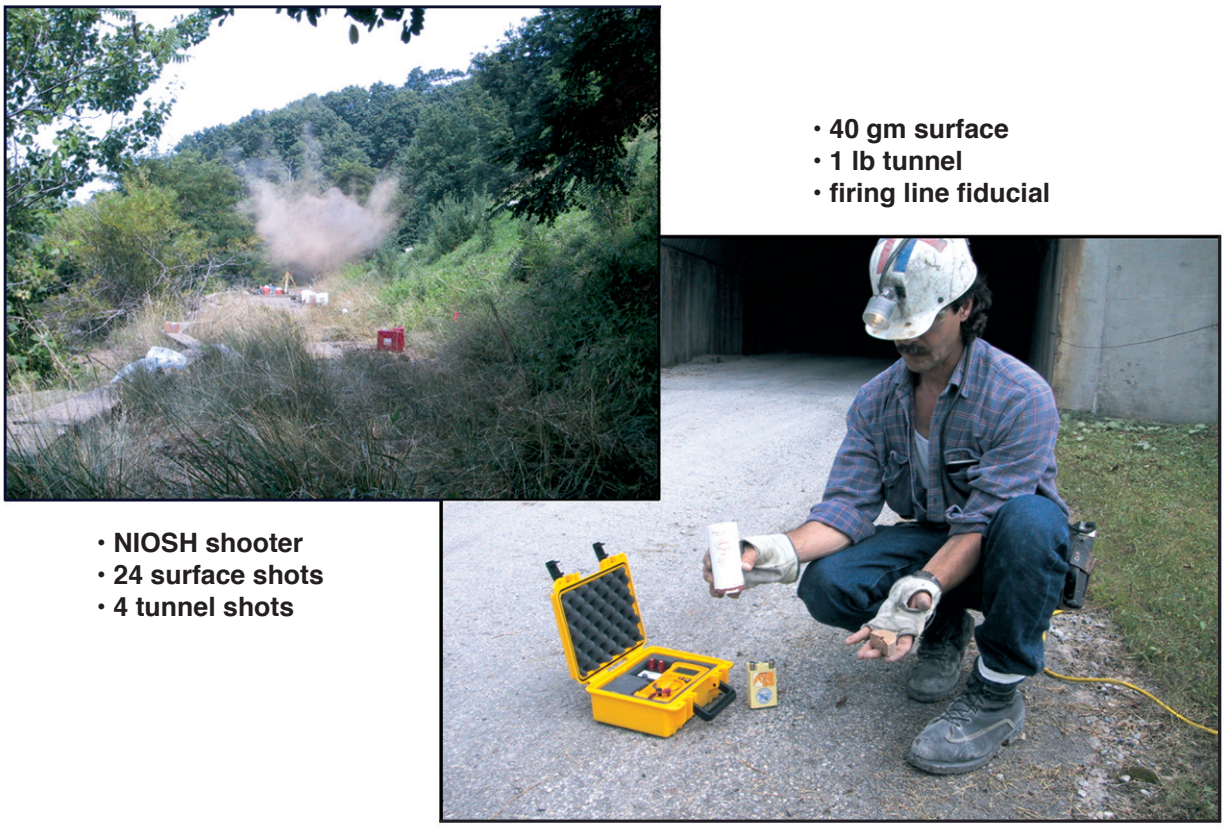

Figure 22. The right photo shows the shooter holding the 40-gm surface charges used in one hand and the 500-gm tunnel shot charges in the other hand. The top left photo shows a typical surface charge detonation.

a few microseconds and not considered an appreciable source of timing error. To maximize battery life and to minimize the amount of data collected, each DAS was programmed to turn on for 5 minutes every half hour. Shooting was conducted within the DAS-on time window. A fiducial (or zero-time) was determined by coiling many loops of the firing line around a designated geophone. The firing signal resulting from the firing box capacitor discharge generates an EMF in the looped wire that the designated geophone responds to. The first peak in the firing signal picked up by the designated geophone was consistently used as the shot fiducial.

Tunnel shots: The tunnel shots were conducted to determine if surface seismic arrays could be used to detect ordnance detonation within a tunnel. There was little doubt that an FK analysis from the surface arrays would point to the source of a single ordnance detonation. The real question was: Can the arrays detect the locations where several detonations occur simultaneously? The data to address this question was gathered as follows: three 500-gm explosions were conducted in three separate locations along the main tunnel followed by a simultaneous detonation of 500-gm explosions emplaced at the same locations. The shots were conducted during the DAS-on time windows.

The tunnel data was checked for consistency by time-shifting and adding the individual shot seismograms to get a fairly good match to the simultaneous shot seismogram. Although such a result is to be expected in theory, concerns on consistent coupling of shots fired successively at the same location necessitated that it be tested. The individual shots and simultaneous shot were analyzed using the same surface seismic array records. The seismograms recorded from an individual geophone of the array and the final results of a broadband FK analysis are shown in Figure 23. The FK results of the single shots all point correctly back to the source location with the bearing accuracy indicated by the figure. The simultaneous shot analysis, however, cannot distinguish between multiple shots. Instead, a single back azimuth with greater variance is produced. It will clearly be a difficult task to distinguish the individual locations in a simultaneous ordnance detonation using this

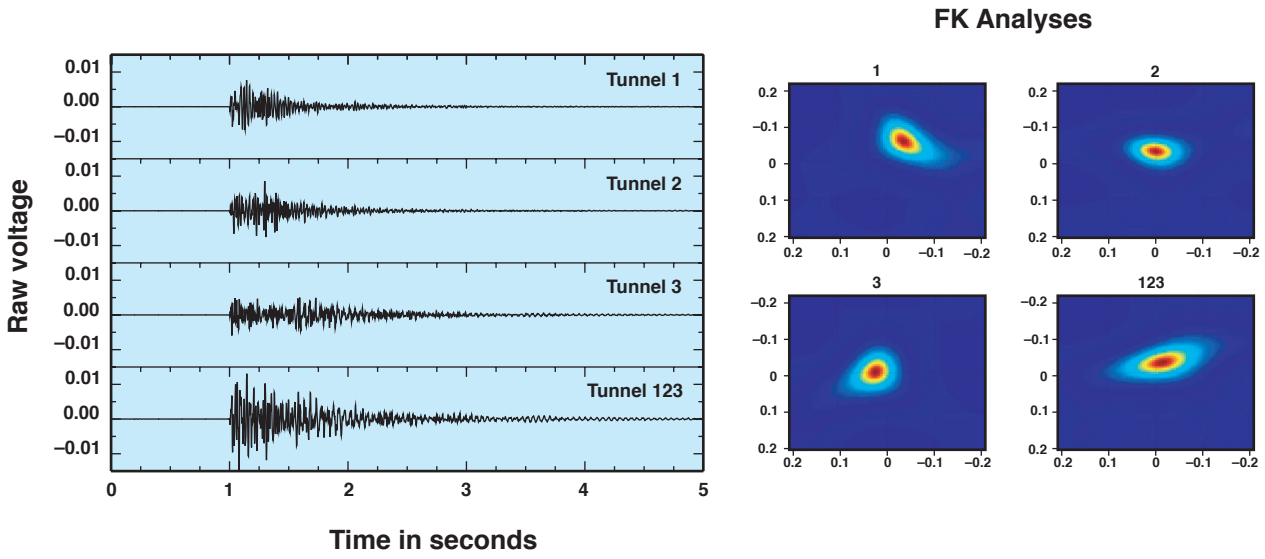

Figure 23. Seismograms of the three individual shots and the one simultaneous shot are shown from one surface geophone located near the tunnel. The right-side FK analyses show good detection and bearing location of individual shots but a "smeared" effect for the simultaneous shot.

method as applied here.
Although the layout of the sensors was not right to test a different approach, there may be an effective way to approach this assuming the general locations are known well enough in advance to lay out the seismic arrays optimally. We noted that an adequate back azimuth could be calculated using the first 100 ms of signal data. A strategic layout of arrays, in many cases, could be accomplished such that for each tunnel shot point there is an array close enough to receive the first 100 ms or so of signal from that shot before the signals from other shots reach the array sensors. In such a layout, individual shots in a simultaneous detonation could be distinguished using FK analysis in a narrow time window on the first arrivals at each array.

Tapping tests: The deployment timing and location of this experiment was close to the Quecreek Mine flood that trapped a number of miners on July 24, 2002, who eventually were rescued four days later. The incident highlighted the need in NIOSH for a new emergency method for locating miners. Although an emergency seismic network-based system designed to locate trapped miners (based on their active tapping, an emergency action they are all trained to do) was set up in the early stages of trying to locate the miners trapped in the Quecreek Mine, the system did not prove effective. The problems centered on deployment difficulties and operation in a high background seismic noise environment (created by the pumping of oxygen into the tunnel complex). The setup of the sensors in an array configuration was ideal for testing an alternate seismic array-based trapped-miner detection system. The analysis of such data is outside the scope of this project, but the necessary data for such an analysis was collected by conducting a scripted series of tapping experiments on the walls and ceiling of the central tunnel during DAS-on time windows. The data was subsequently shared with NIOSH and also proved useful in determining bulk seismic velocity properties

Full 3D

The Lake Lynn experiment was conducted in a region of complex 3D features that had to be accounted for in modeling. The proximity to the highwall meant that reflections off the highwall would occur and needed to be adequately modeled. In addition, the steep topography meant that the tunnel depth grew significantly, from about 80 ft at the highwall face to over 200 ft at the farthest upslope array location from the highwall. Accurate accounting of topography in the model was crucial. Another feature that was critical to get right in the modeling and that was shown to play a major role in signal characteristics of the recorded data was the surface weathered layer. In analysis of the Lake Lynn recorded data it was noted—particularly in analysis of the tapping tests—that some arrays consistently recorded P-wave arrival times on particular geophones earlier despite a longer path. What is important in this finding is the amount of delay (1 to 2 sample points or 2 to 4 ms) observed. The timing error of geophones recorded by the same DAS is just a few microseconds, the error in surveying is centimeters, and the paths followed from the signal source to the array through the formation are nearly identical. The observation can only be explained by variable delays encountered in a variable thickness weathered zone of very low seismic velocity. This low-velocity layer varied in thickness along the hillside from 0 to about 5 m in thickness. Unfortunately, no map of the layer thickness with position exists, and hence we had to make simplifying assumptions. In the first model developed, a 3-m-thick low-velocity surface layer was draped evenly over the entire model including the highwall. This was a simplifying assumption that did not reflect the actual geology, particularly on the highwall and on the highwall bench that extended some 5 m between the vertical wall and the beginning of the hill slope. The simplification made the first model much easier to construct and it was not clear at the outset that such an assumption would have a major effect on the wavefield results. The first model was produced using Earthvision and consisting of 32 million nodes is shown in Figure 24.

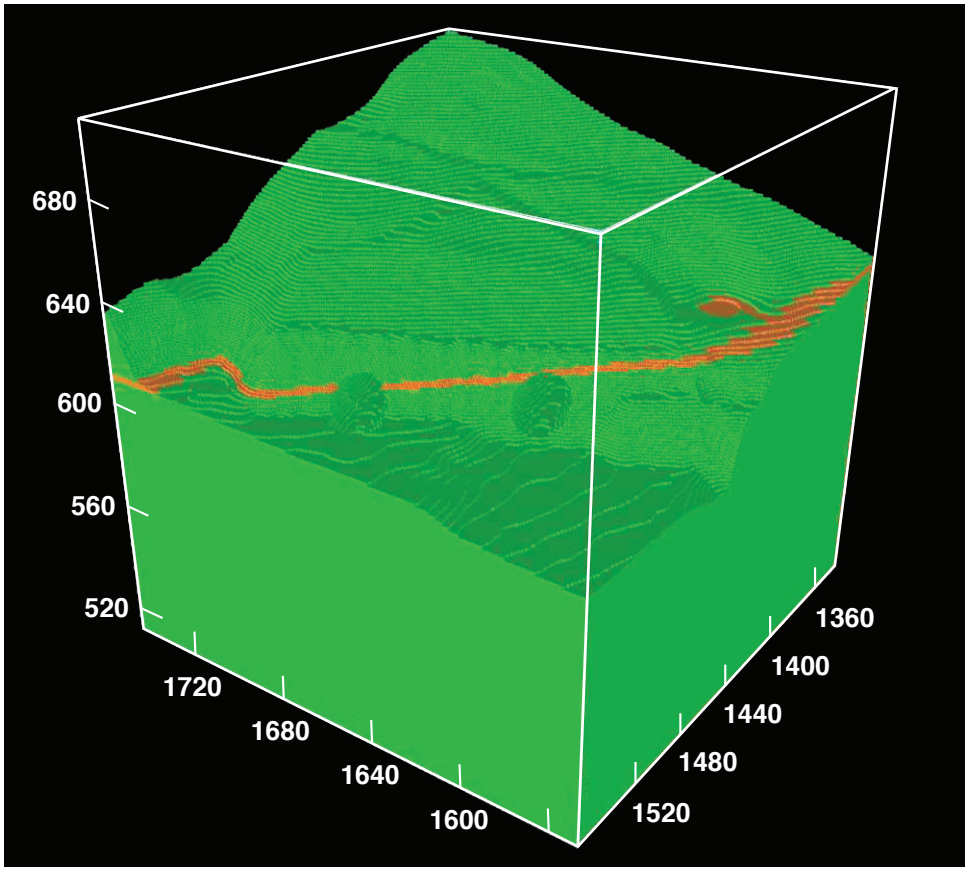

Figure 24. The topography and two tunnels are shown in the 3D plot along with an orange colored lithologic layer to illustrate the geologic stratigraphy.

Significant effort was spent in adapting the model output produced by Earthvision to a form accepted by E3D. E3D runs were accomplished for the above model and for the model without the tunnels. The run duplicated an experimental shot at the farthest upslope location along the axis of the primary (leftmost facing headwall) tunnel, comparing seismograms of the simulation with and without the tunnels. The wavefield for that shot is shown in Figure 25 as successive snapshots in time as the seismic energy spreads from the shotpoint. When individual seismograms were compared between this simulation and an identical simulation without the tunnel complex the differences showed less than a 1% difference in the broadband amplitudes of the seismic record during times reflected phases were present. The planned analysis methodology using simulated data spanning uncertainties in geology to match against field data probably has errors in excess of 1%, and hence it is unlikely that it would be successful if the model comes close to reflecting reality.

The complexity of the geological environment coupled with 3D effects is best seen in the difference images presented in Figure 26. The difference images represent the signal differences over time between the tunnel-in simulations and simulations without a tunnel. The images can be thought of as the tunnel-reflected signal only. Note that this is simulated data and that the percentage differences between the tunnel-in and tunnel-out signal amplitudes is only about 1%, which was not a large enough difference to be discriminated in the field data. The images show the evolution of the tunnel-reflected signal with time and the significant complexity of the signal as it reflects off the highwall and other structures.

The wavefield results from the first model suggested that a better, more realistic model was the logical next step in understanding the scattered tunnel signature. The second-generation model was developed after simulations from the first showed very little tunnel-reflected wave energy detectable by

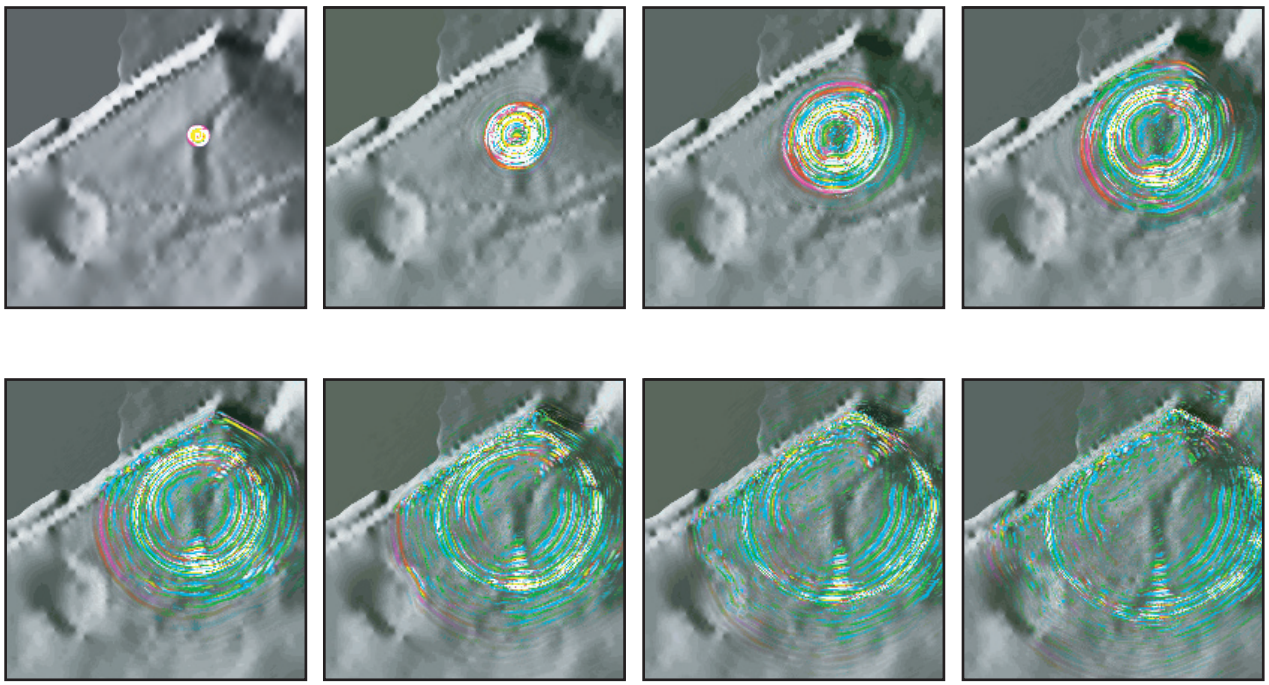

Figure 25. Successive wavefield time history snapshots in map view for a shot location that is identical to a field test shot. Magenta color is P-wave energy, turquoise is S-wave energy.

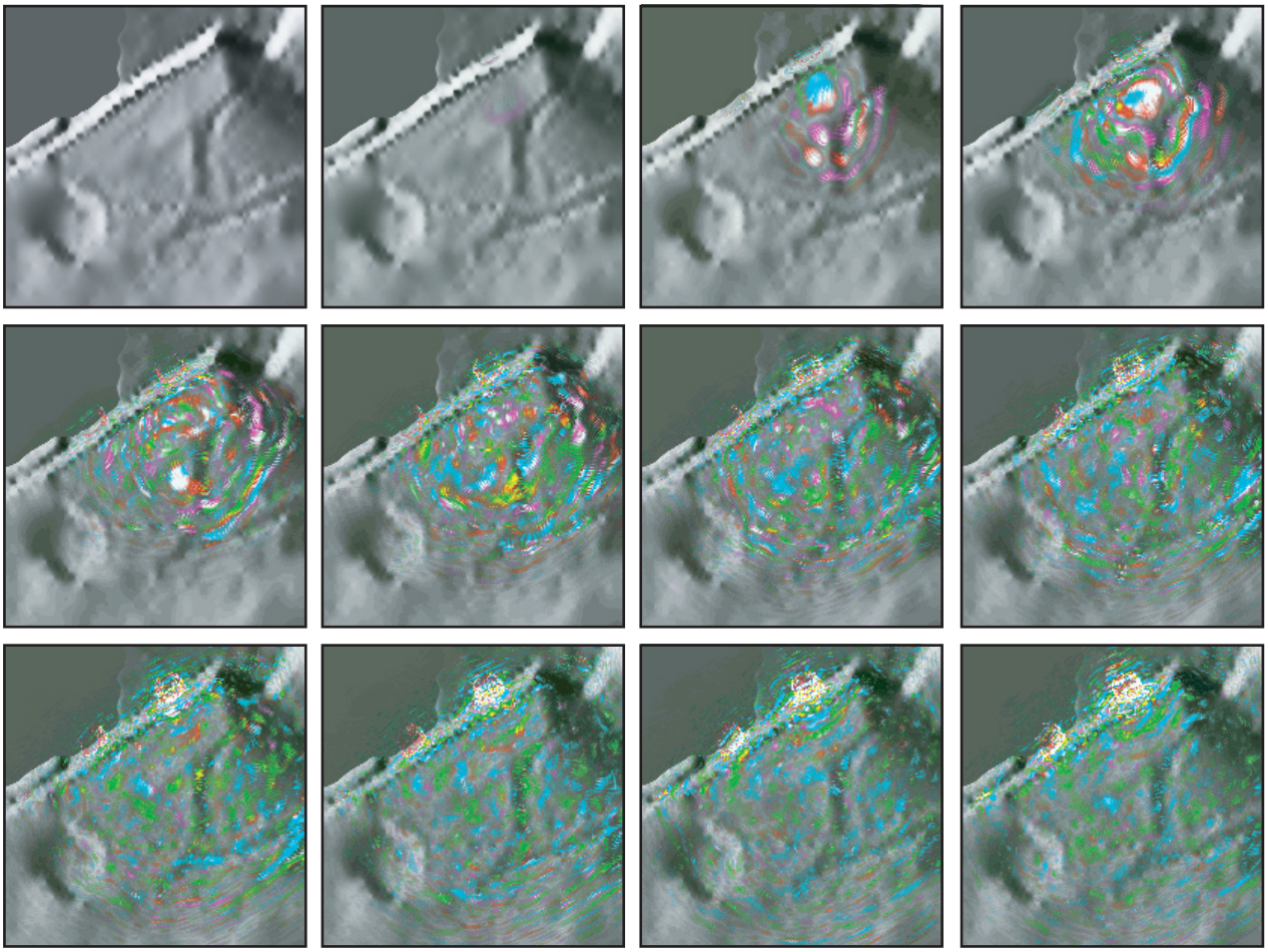

Figure 26. Successive time history snapshots of the difference wavefield in map view where magenta is P-wave energy and turquoise is S-wave energy. The difference wavefield is the tunnel-in wavefield model subtracted from the tunnel-out wavefield model. It is essentially the tunnel scattered wavefield.

surface-mounted sensors. When synthetic seismograms were produced for hypothetical sensor locations below the weathered layer, the tunnel-reflected signal amplitude grew appreciably. During the experiment, two arrays were partially mounted on a flat bedrock bench that extended about 5 m in from the highwall before the steep slope and weathered layer are encountered. Since we had sensors mounted on bedrock to compare with, we increased the complexity of the model by terminating the weathered layer 5 m before the highwall. A more accurate lithology was also used in the second model. E3D was used to create synthetic seismograms at the same locations as the bedrock sensors. The second model is shown in Figure 27.

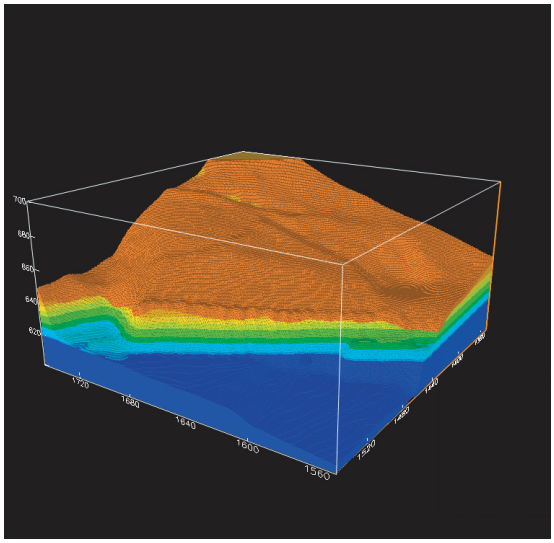

Figure 27. Final model of the Lake Lynn field site used in E3D wavefield calculations.

The final 3D geologic model of the Lake Lynn mine site consists of 9 stratigraphic units that were mapped along the steep cliff face at the main portal. These units, from the surface to the base, are as follows:

Lithology	Thickness	Strength
1) Weathered layer	1-5 m	very weak
2) Highwall top	----	----------
3) Weathered limestone	>1.5 m	moderate
4) Thin-bedded shale claystone	>3 m	weak
5) Limey shale/ shaley limestone	3 m	moderate
6) Massive limestone	3-5 m	strong
7) Limey shale/ shaley limestone	<3 m	moderate
8) Massive limestone	4.5 m	strong
9) Thin-bedded shale	<1 m	weak
10) Massive limestone	>6 m	strong

The thickness of each unit was visually estimated, since access was restricted near the high wall cliff. The rock strength was interpreted from the visible weathering patterns. Some of the rocks were also inspected inside the mine.

The surface topography was constructed using survey data provided by the Lake Lynn Laboratory. A CAD file containing the locations of cultural features, as well as the tunnels, was also provided.

The 3D geologic model was constructed using software called Earthvision v. 7.0 (Dynamic Graphics, Inc.). A regularly-spaced 2D grid is created for the surface of each stratigraphic unit. Since there was very limited borehole data available, we assumed an attitude for each surface and projected this grid into the hillside. This strike and dip are based on the regional attitude established in this area and provided to us by the personnel at the Lake Lynn site for this tunnel complex. The topographic surface is also represented as a 2D grid. The thickness of the weathered surface layer is not known, so a second grid was created below the topographic surface and this grid mirrored the topography. The volume between these 2 grids represents the weathered layer.

At the time that this model was created, we had a version of Earthvision that could handle only small 3D grids (since then, we purchased the extended version, which will handle any size grid). Thus we had to devise a way to get around these limitations, and with the help of DGI, we came up with a script that generated a “dummy” 3D grid in the formula processor, with the specified grid interval of 0.5 m. This grid contains 32,000,000 NULL nodes. The grid of NULL values is “sliced” by each structural surface (a 2D grid) and all nodes that are located above and below this surface are assigned a unique index value. Each stratigraphic surface cuts completely through the model. The resulting 3D grid contains no NULL values, but rather nodes with index values based on which stratigraphic unit occurs between the surfaces. The void (air) above the topographic surface is also assigned a unique value. Physical properties are linked to the index values.

The tunnels are represented as line segments through the model. Nodes within a specified radius of each line segment are converted to NULL values. The resulting regular 3D grid is exported to a scattered ASCII data file. The NULL values representing the tunnels are then converted to a unique value of “-1”. This file is undergoes additional manipulations prior to use by E3D.

The synthetic seismograms for selected sensor locations of the two arrays that are partially located on the bedrock bench were compared

for tunnel-in and tunnel-out simulations given a shot location upslope and just off the main tunnel axis. The comparison of sensor elements on the bedrock and in the weathered zone are compared in Figure 28. The figure shows very little difference in the signal amplitude and features between tunnel-in and tunnel-out seismograms. This is true for sensors on the bedrock as well as sensors in the weathered zone. The model gives little hope for detecting such small differences in the data. It should be noted that the synthetic data showed larger changes at frequencies between 100 and 200 Hz, but since we observed little energy at these frequencies in the field data we also did our analysis of data and simulations in the 50- to 100-Hz band.

Since simulations showed the tunnel influence on the recorded waveform to be very small, even for the sensors on bedrock, observing such differences in the data using the full analysis methodology would not be likely. To determine if the weathered zone was playing a significant role in obscuring the tunnel signal by attenuating and scattering the source energy, simulations were conducted with the source at 5-m depth, well below the weathered layer and in competent bedrock. The results are shown in Figure 29.

The figure does show a more pronounced effect and highlights that it is important to get the source below the weathered layer to have a chance of observing the tunnel scattered wavefield. The figure also shows that in the 50- to 100-Hz band, the signal differences are smaller, particularly for a soil-mounted sensor.

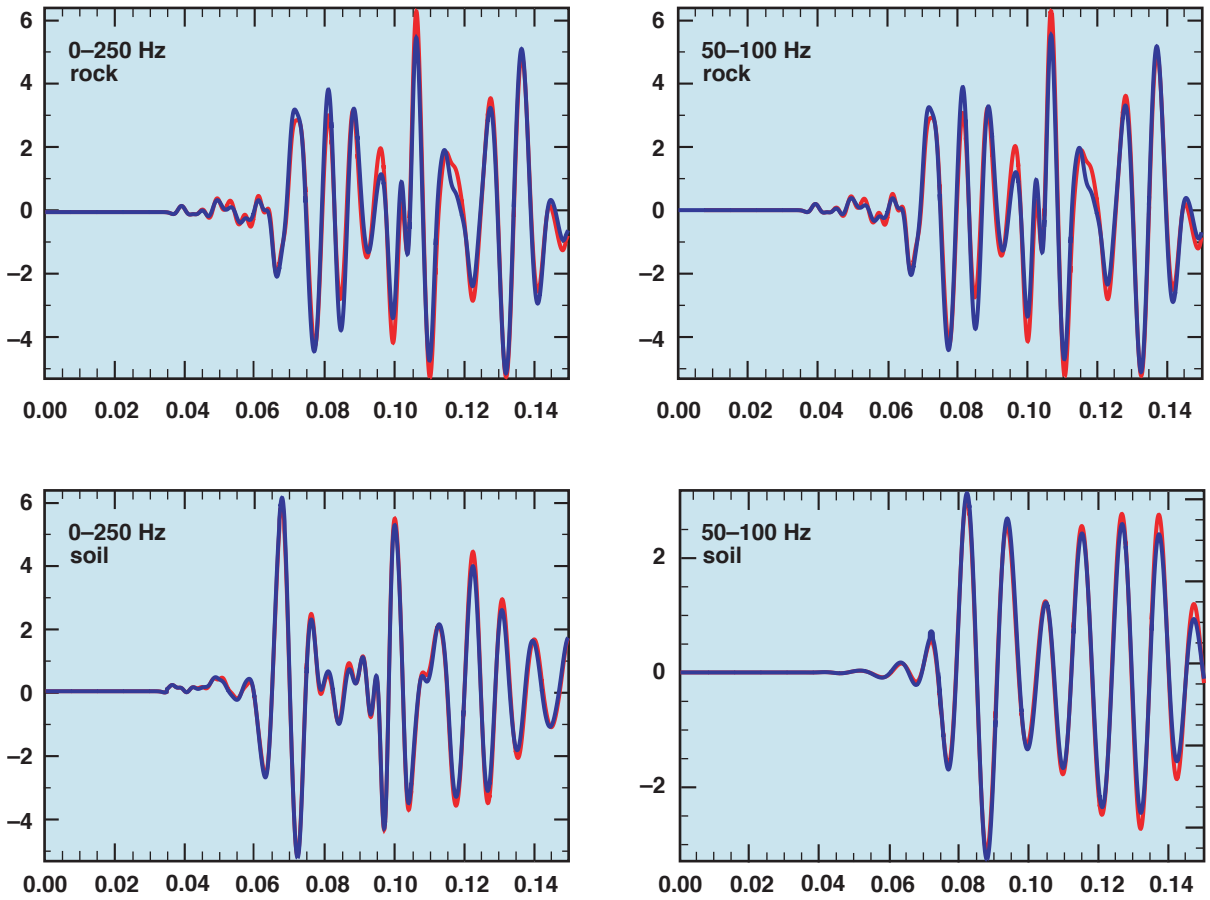

Figure 28. A comparison of tunnel-in (red) synthetic seismograms with tunnel-out (blue) synthetic seismograms for an identical shot upslope and just off the tunnel axis. The top row of plots is for an array sensor mounted on the bedrock bench. The bottom row is for a sensor from the same array that is mounted upslope in the soil layer. The plots to the right are bandpass filtered versions of the plots on the left.

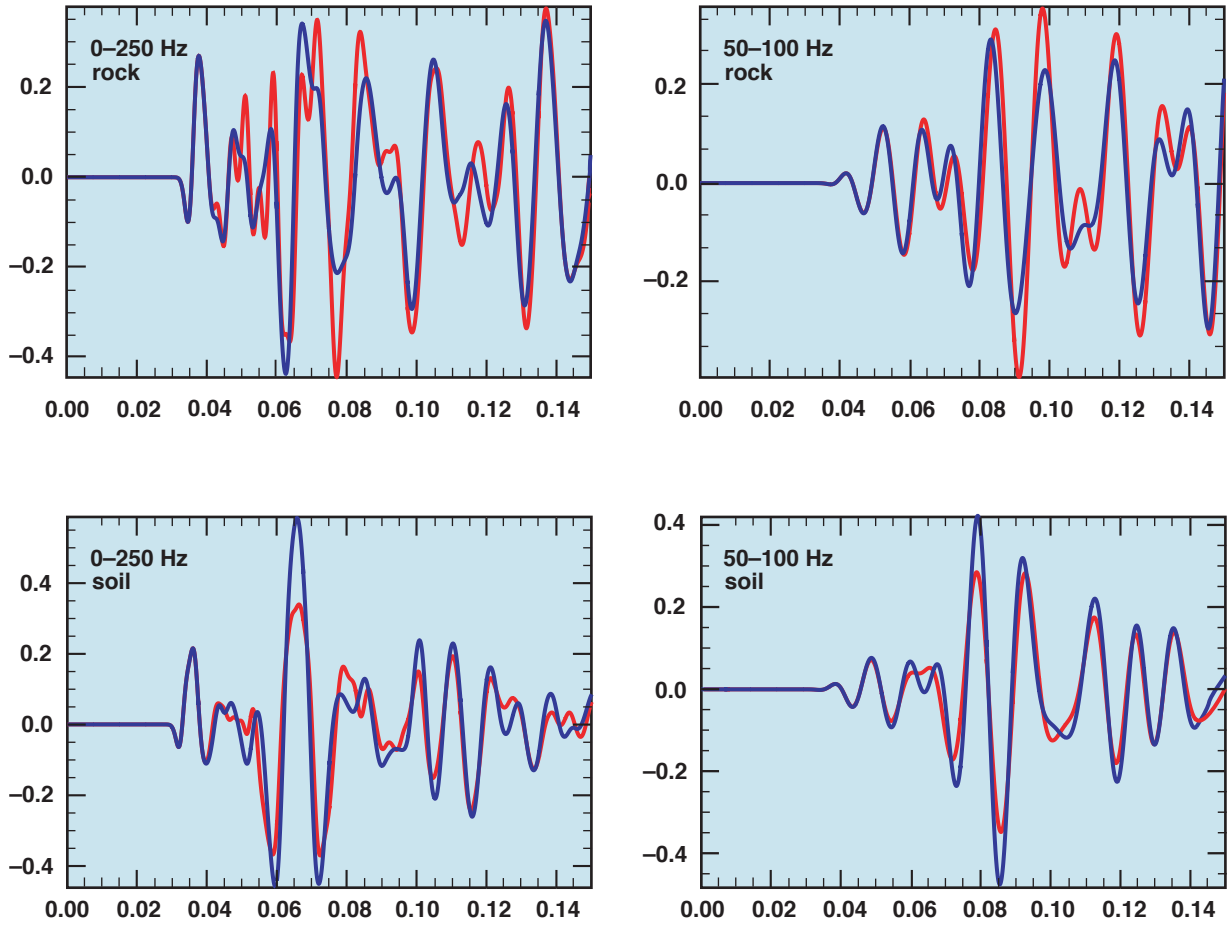

Figure 29. Same sensors and shot as the previous figure with the source buried 5 m below the surface in competent bedrock. Note the larger relative differences compared to the previous figure.

Although the field data shows significant energy in the 50-100 Hz band and little energy above 100 Hz, the simulation data has good signal-to-noise above 200 Hz since a noise component was not input into the simulations (although frequency-dependent attenuation was). Since reflected energy off a tunnel will be more pronounced for wavelengths on the order of the tunnel dimensions then, given the test site tunnel dimensions and bulk body-wave velocities in the immediate vicinity, reflected energy will be most apparent at frequencies above 100 Hz. Unfortunately, there is insufficient signal-to-noise in the field data above 100 Hz. The simulation data, however, can be used to qualitatively assess the expected tunnel-reflected signal at optimum frequencies (100-200 Hz).

Figure 30 shows the relative differences in amplitude between the tunnel reflected signal only (red) and the direct signal (black) 0.5 meters from an upslope shot along the tunnel axis. The vertical scale difference between the two plots is about 1000. This illustrates the difficulty in detecting the tunnel reflection near the shot and how important it is to arrange a source-receiver geometry that keeps the surface wave energy and tunnel signals from time coincident arrival. In this case, the surface wave energy is well past the receiver before the tunnel-reflected signal arrives.

Single point comparisons of models with and without the tunnels present can be made for

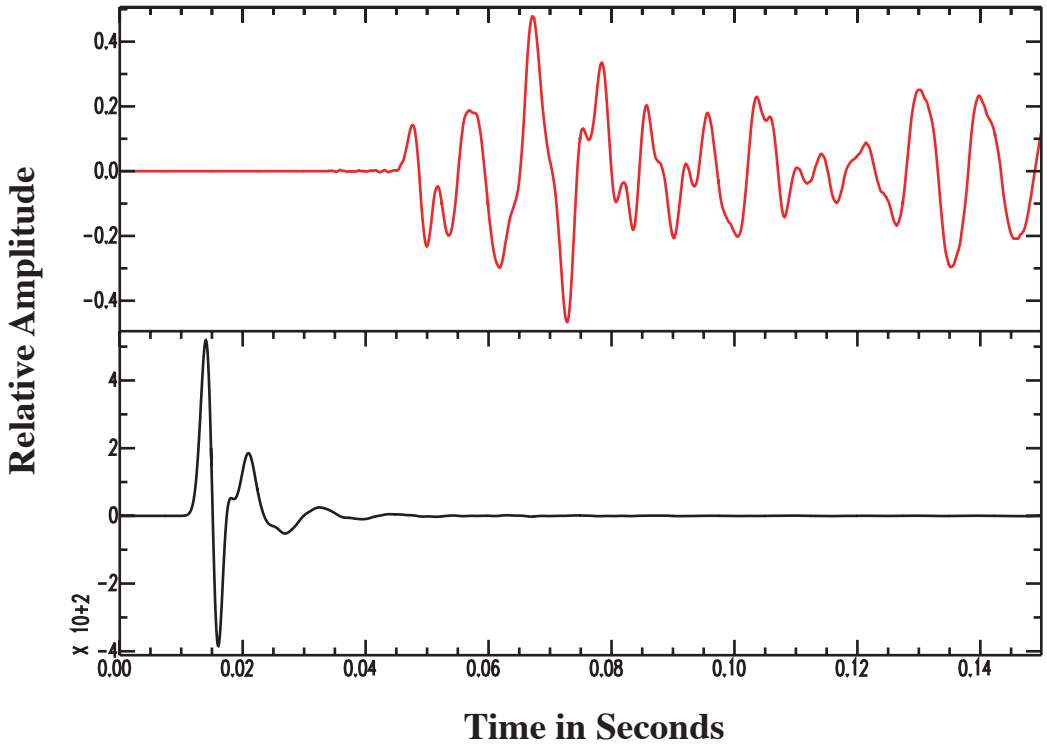

Figure 30. Comparison of the simulated shot seismic signal recorded at .5 meters from the source (black) with the tunnel-reflected signal recorded at the same location. The tunnel-reflected signal is about 0.1% of the surface wave amplitude.

other sensor positions to see if a tunnel-reflected signal could possibly be seen in the field data. Many comparisons with the simulated data have shown that we cannot expect to find a tunnel-reflected signal in the field data for frequencies below 100 Hz. If we restrict the following analysis to the frequency band 100-200 Hz, and look at favorable source-receiver geometries, a tunnel-reflected signal is visible in the simulation wavefield. Figure 31 shows the model simulation at a location along the tunnel axis close to the highwall for the same upslope tunnel axis shot. This figure shows the modeled seismogram at that sensor location (black) along with the tunnel signal only (red) which was computed by differencing the model runs with and without tunnels present. The early part of the waveform is dominated by low amplitude body waves; the initial arrivals are direct body waves from the shot (black). The following few cycles are the tunnel reflection signal, evidenced by the red and black traces nearly overplotting. The later arriving tunnel scattered signal is then overwhelmed by the large-amplitude surface wave arrival. It would be very difficult to isolate the tunnel signal in the surface wave seismogram.

The above discussion does show that, for the right frequency band, the right source-receiver geometry, and observation within the right time window, it is possible to observe the tunnel reflected signal in the seismogram. This emphasizes the need for a detailed wavefield analysis of any potential field site to determine if a signal can be observed and how sensors, shots,

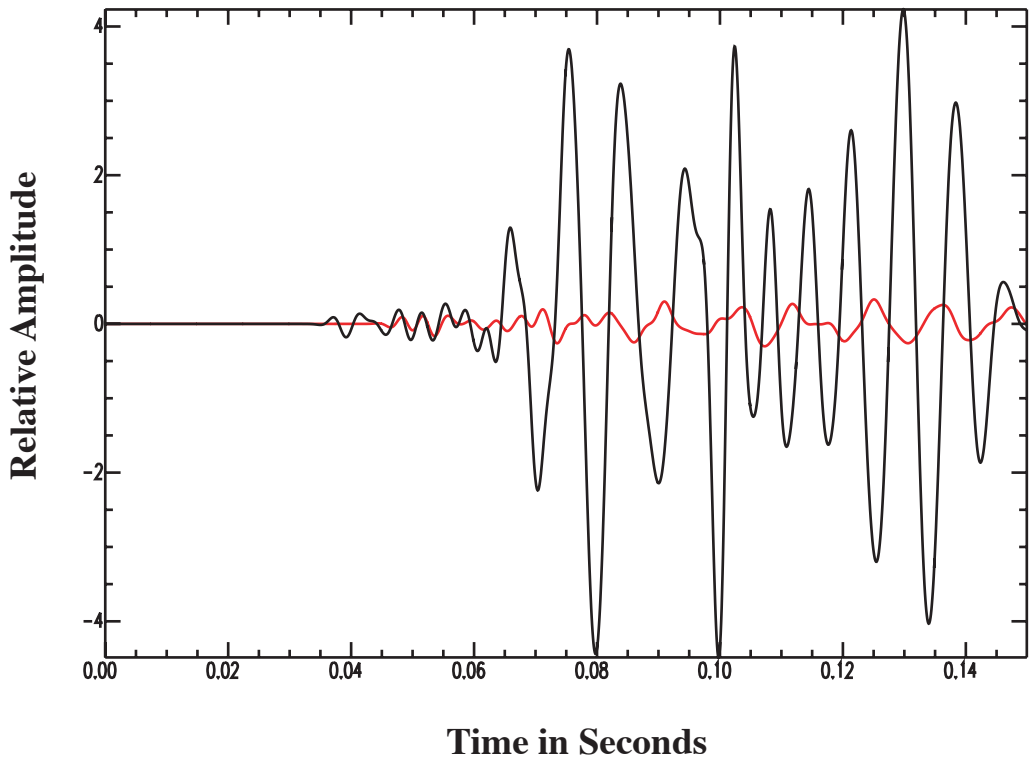

Figure 31. Simulation comparison of the tunnel only signal (red) with the full waveform (black) at 100-200 Hz.

and analysis windows should be arranged prior ti field data collection.

Figure 32 emphasizes that although a tunnel reflected signal can be observed in the simulated data, it could easily be confused with other signals arising from geological complexity. That figure is identical to figure 31 except the location is 40 meters from the tunnel axis and hence should see a much weaker tunnel signal. Indeed, the early body wave arrivals are similar to the previous figure however, the observed waveform features in the black curve are not the result of the tunnel signal as evidenced by the relatively flat smooth tunnel signal curve (red). The point here is that although the body wave seismogram features of figure 31 are dominated (in a small time window) by the tunnel signal but are not in figure 32, it would be very difficult to say, looking at the black curves only, which is dominated by a tunnel reflected signal and which is not.

As was noted in the simulation experiment, the tunnel reflected and scattered signal is complex and strongly influenced by geological heterogenity. To determine if different phases could be identified in the tunnel signal, a profile along the tunnel axis was created from the difference of the tunnel-in and tunnel-out geological models using the wavefield simulations. The profile extends from the upslope shot on the tunnel axis along the tunnel axis to a point just short of the highwall. Seismogram differences are calculated at every half meter along the profile, 50 traces in all. Figure 33 shows the tunnel signal profile in the 100-200 Hz band. Though not shown here, the profiles

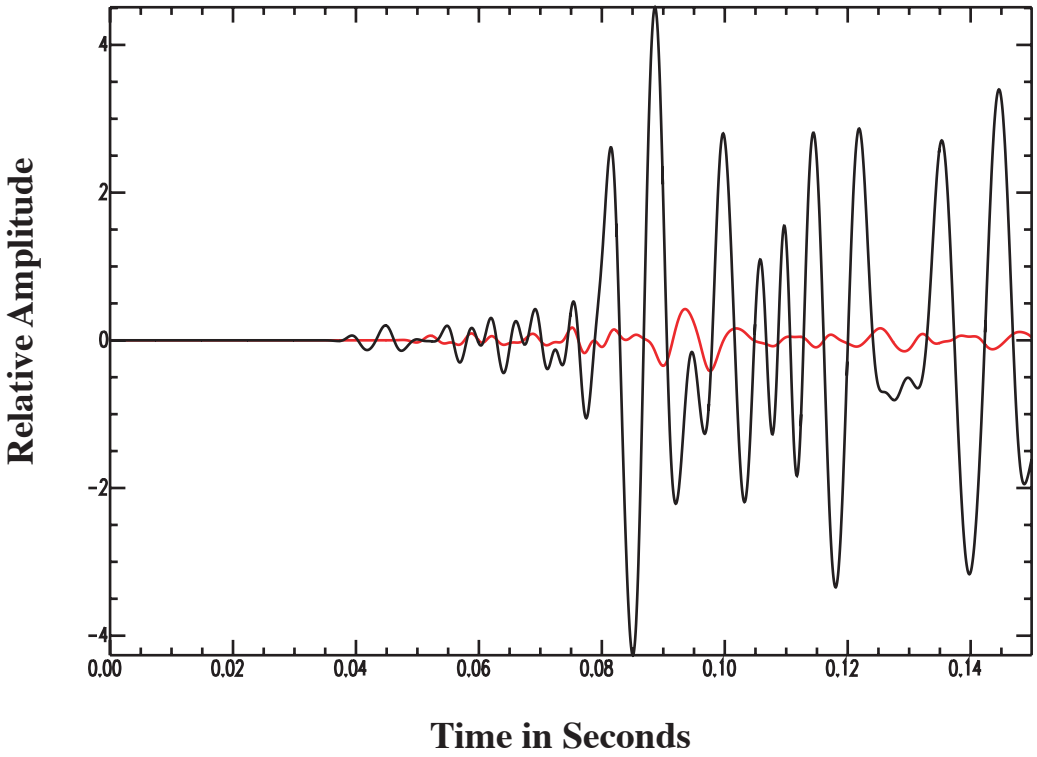

Figure 32. Off tunnel-axis comparison of the tunnel only signal (red) and the full waveform (black).

of both the tunnel-in and tunnel-out models show numerous distinct phase arrivals associated with the direct body wave path, tunnel reflected path, and surface wave phase. The profile shown in the figure only exhibits one distinct phase arrival throughout the profile, the initial tunnel reflected phase. Although other phases could be anticipated, such as reflections off the highwall both before and after the tunnel reflection, such phases are not consistent across the profile and therefore cannot be clearly associated. It should be noted that the same profile in the 1-100 Hz band does not exhibit any consistent phase arrival across all traces. This is consistent with expectations for scattering of seismic energy by anomalies that are significantly smaller than the seismic wavelengths.

Many attempts were made in comparing field data to the simulations. As noted earlier, the tunnel reflected signals could not be compared because insufficient high frequency energy was observed in the field data. The lack of high frequency energy (100-200 Hz) is due to an attenuating surface weathered layer and to background noise. Direct comparison of field seismograms and simulations did show general agreement in body wave and surface wave arrival times. The 50-100 Hz band was found to be the best for comparing simulation results to field results, however, close matches of the waveforms did not occur for sensors located on the weathered layer. The weathered layer was found to be very attenuating and highly variable in thickness, consequently the uniform thickness used in the model resulted in significant errors. Fortunately, some sensors were located on the highwall bench and coupled to bedrock. These

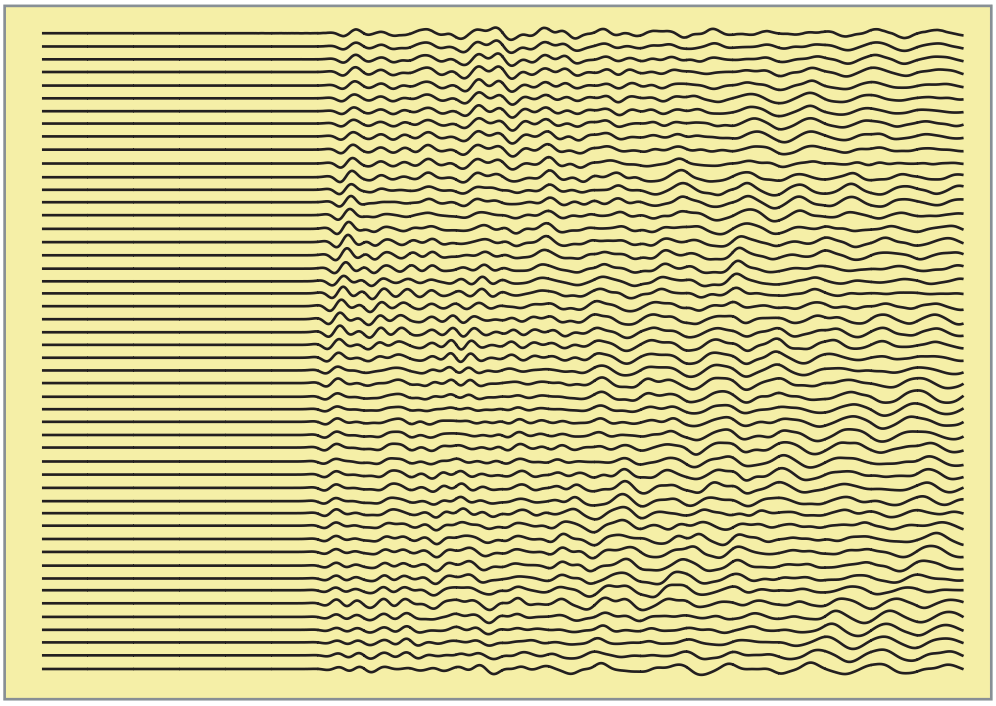

Figure 33. Profile section, tunnel signal only, for an upslope tunnel axis shot from shot (top) to highwall (bottom) in 0.5 meter increments. Only the first tunnel reflection arrival shows good correlation across all traces.

seismograms were found to be good agreement with the simulations seismograms.

Figure 34 shows two comparisons of simulated results against actual field data. The top comparison is at a sensor location on the bench near the highwall and along the tunnel axis for an upslope shot along the tunnel axis. The similarity of the waveforms, dominated here by surface waves, is apparent. The bottom comparison is for the same shot but at a sensor location well away from the tunnel axis but on the bench near the highwall. The waveform features are clearly similar but these are surface wave features that dominate. We conclude that we can model a complex 3D structure and provide fairly accurate surface-wave wavefield models in the absence of a weathered layer but accounting for topography and complex geology and geometry. Unfortunately, we did not have sufficient high frequency in the field data to compare body wave simulations with the field data and consequently cannot say if the body wave simulations are as accurate.

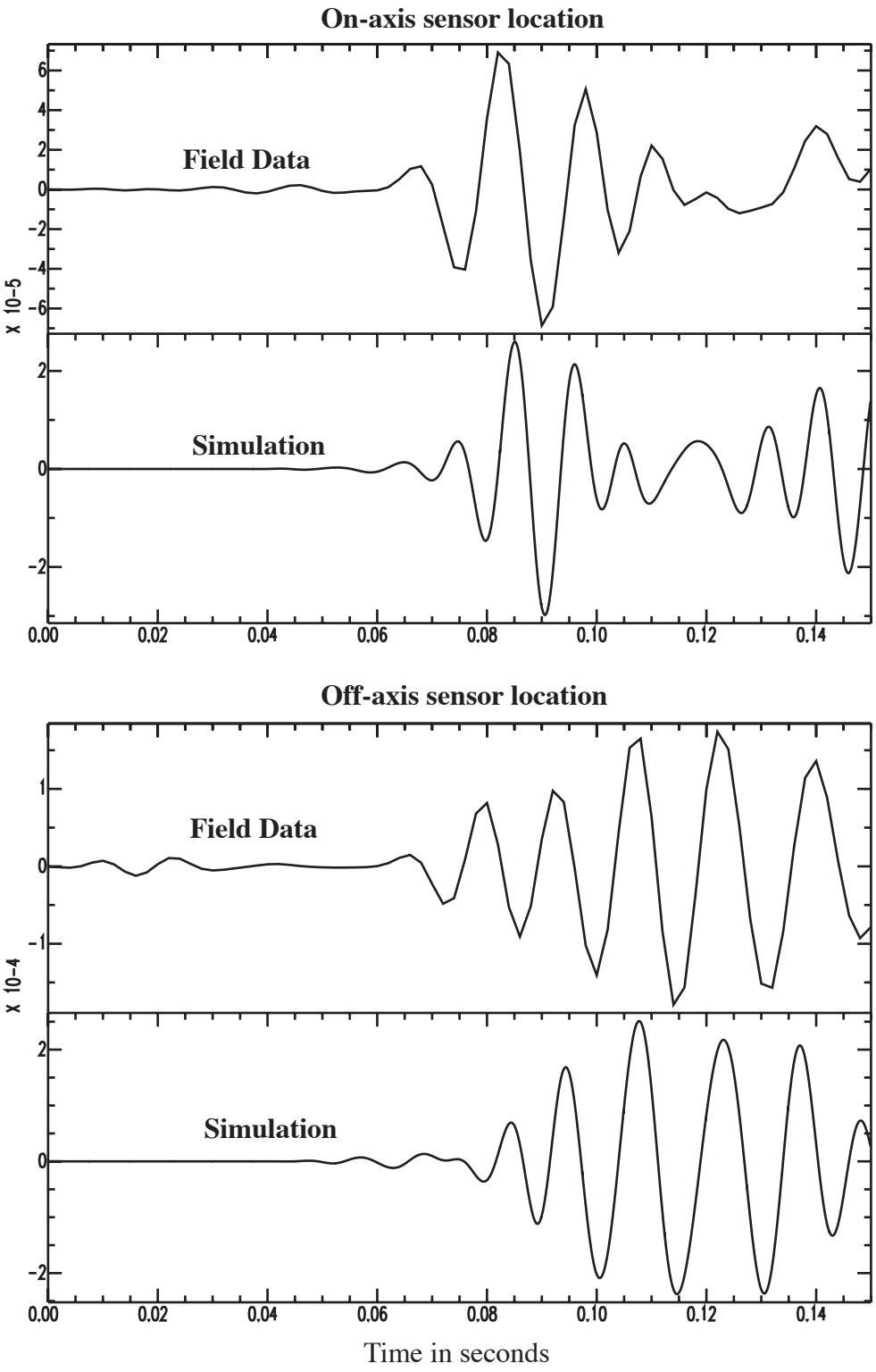

Figure 34. Two field data-model comparisons: a sensor located on the bench along the tunnel axis (top) and and off-axis bench location some 40 meters from the first (bottom). The waveforms have been band passed between 50 Hz and 100 Hz with surface waves dominating the records.

Conclusion

The capability-building technical developments resulting from this project have resulted in new applications and opportunities. The enhancement of E3D to account for topographic effects on the wavefield calculations have resulted in new applications of E3D on smaller-scale problems where topography effects become significant. The development of wireless technology, in particular, the telemetry of seismic data to a central web-enabled processing system is virtually complete. This development will enable real-time seismic vehicle tracking systems using the matched field paradigm explored in this project. The K-L statistical methodology for characterizing geological heterogeneity shows great promise as a robust and flexible means to bound the uncertainties in physical properties tied to geological structure and may be an important tool in development of other stochastic optimization search methods currently under study.

The project has been successful in demonstrating that the matched field processing approach to the vehicle tracking problem, using calibrated field data, was effective and could be the basis for development of an operational system.
The project has also been successful in demonstrating the validity of the approach of using matched field processing and sophisticated forward modeling coupled with statistically generated geological heterogeneity to select among alternate underground facility layout hypotheses. The approach was validated with the simulation experiment that concluded that spanning geological uncertainties improved statistical performance and accuracy of the methodology. The simple deployment over a shallow tunnel at NTS showed a significant reflected signal could be observed and utilized under ideal conditions [shallow depth (20–50 ft) and competent rock to the surface]; however, a full-blown realistic experiment that included strong 3D effects, relatively deep burial depths (80-200 ft), and an attenuating surface layer did not produce observable reflection signals and could not be used in an experimental validation of the processing methodology. That said, the demonstration of modeling the full complexity of the 3D geology and running E3D to get the complex wavefield was a success in itself. The results showed good fit to the field data in the 50- to 100-Hz bandwidth and point the way to follow-on studies based on E3D to decide via modeling which particular field sites could return reflected signals of sufficient amplitude for our processing methodology to be applicable.

The Lake Lynn experiment did produce other results of significance and identified a number of potential spinoff projects. Single-point ordnance detonation could be located by arrays, but simultaneous multiple-point detonations require a strategic layout of arrays based on a priori knowledge of the detonation points. Small-aperture seismic arrays could be an effective approach to a new-generation seismic detection and location system for trapped miners featuring a movable, quickly deployed system with real-time FK analysis. The general concept of deployment planning based on intensive forward modeling so that analysis and decisions can be made rapidly can be applied to other geophysical surveys, such as gravity.
The final benefit of this project was the interaction with potential new sponsors it provided and the formation and development of new collaboration partners, such as NIOSH, that it produced. Briefings and discussions with potential sponsors have helped us understand current sponsor needs and issues and have identified a number of Lab technologies, well beyond the scope of this effort, that could be applied to potential sponsor problems.

Acknowledgments

Numerous agencies and individuals helped with the developments described herein. The Nevada Army National Guard supplied tanks for the Nevada Test Site tracking experiment. The National Institute of Occupational Safety and Health through the Lake Lynn Laboratory supplied a tunnel test site and supported our activities. Mike Sapko of NIOSH was essential to our successful data collection there. At LLNL, Bruce Henderer developed the wireless seismic communications; John Futterman conceived of the on-site vehicle tracking testbed; Pat Lewis and Don Rock provided field support to all experiments conducted over two years. Bruce Jahn conducted all surveys at the Lake Lynn facility and Dominic Griggs provided graphical rendering of the site survey data.

References

Fialkowski, L.T., M.D. Collins, W.A. Kuperman, et. al., *Matched-field Processing Using Measured Replica Fields*, Journal of the Acoustical Society of America 107(2), pp 739-746, 2000.

Larsen, S., and J. Grieger, *Elastic modeling initiative: 3-D computational modeling*, Soc. Expl. Geophys. Proceed., 68, 1803-1806, UCRL-JC-130224, 1998.

Van Trees, H. L., *Detection, Estimation, and Modulation Theory - Part 1,* pp 178-186, John Wiley & Sons, 1968.